

Signal transduction and directional sensing in eukaryotes

Varunyu Khamviwath¹, Hans G. Othmer^{1,2,*}

1 School of Mathematics, University of Minnesota, Minneapolis, Minnesota, U.S.A.

2 Digital Technology Center, University of Minnesota, Minneapolis, Minnesota, U.S.A.

* **E-mail: othmer@math.umn.edu**

Abstract

Control of the cytoskeleton and mechanical contacts with the extracellular environment are essential components of motility in eukaryotic cells. In the absence of signals, cells continuously rebuild the cytoskeleton and periodically extend pseudopods or other protrusions at random membrane locations. Extracellular signals bias the direction of movement by biasing the extension of protrusions, but this involves another layer of biochemical networks for signal detection, transduction, and control of the rebuilding of the cytoskeleton. Here we develop a model for the latter processes that centers on a Ras-based module that adapts to constant extracellular signals and controls the downstream PI3K-PIP₃-based module responsible for amplifying a spatial gradient of the signal. The resulting spatial gradient can lead to polarization, which enables cells to move in the preferred direction (up gradient for attractants and down-gradient for repellents). We show that the model can replicate many of the observed characteristics of the responses to cAMP stimulation for *Dictyostelium*, and analyze how cell geometry and signaling interact to produce the observed localization of some of the key components of the amplification module. We show how polarization can emerge without directional cues, and how it interacts with directional signals and leads to directional persistence. Since other cells such as neutrophils use similar pathways, the model is a generic one for a large class of eukaryotic cells.

Author Summary

Eukaryotic cells move in response to extracellular signals in a variety of contexts, including the immune response, the formation of vascular networks during development, and metastasis of tumor cells in cancer. The transduction of extracellular signals into changes in the cellular cytoskeleton, which is an essential component of directed movement, is a complex process that involves several layers of control that we partition into modules based on the biochemical steps and their purpose. To enable cells to respond to a wide range of signals cells detect changes in the signal and ignore constant background signals, and this is encapsulated in a Ras-based module in our model. However, extracellular signals are frequently weak, and therefore reliable control of the motile machinery requires amplification of the extracellular signal, and this is performed by an application module based on PI3K, a protein kinase that controls the phosphorylation of certain membrane lipids. The model can replicate much of the observed response of the cellular slime mold *Dictyostelium* to changes in cAMP, which is the signaling molecule.

Introduction

Cell and tissue movement is an integral part of many biological processes, such as large-scale tissue rearrangements or translocations that occur during embryogenesis, wound healing, angiogenesis, and axon growth and migration. Individual cells such as bacteria migrate toward better environments by a combination of taxis and kinesis, and macrophages and neutrophils use these same processes to find bacteria and cellular debris as part of the immune response. Our understanding of signal transduction and motor control in flagellated bacteria such as *E. coli* that move by swimming and bias their movement by control of their run lengths is quite advanced [1] compared with our understanding of how amoeboid cells such as macrophages crawl through tissues. The fundamental issues in the latter context include how directional information is extracted from the extracellular signals, how cells develop and maintain polarity, how cells exert traction on their environment, and how adhesion to substrates or other cells is controlled.

The cellular slime mold *Dictyostelium discoideum* (Dd) is an amoeboid cell that is widely-used as a model system for studying signal transduction, chemotaxis, and cell motility. After starvation triggers the transition from the vegetative to the aggregation phase, Dd uses 3'-5'cyclic adenosine monophosphate (cAMP) as a messenger for signaling by pacemaker cells to control cell movement in various stages of development [2]. The production and relay of cAMP pulses by cells that are excitable but not oscillatory, coupled with chemotactic movement toward the source of cAMP, facilitates the organization of large territories. In early aggregation the cells move autonomously, but in late aggregation they form connected streams that migrate toward the pacemaker (reviewed in [2]).

Cell motion in Dd consists of the alternating extension of pseudopods and retraction of trailing parts of the cell [3]. Not all extensions are persistent, in that they must anchor to the substrate or to another cell, at least temporarily, in order for the remainder of the cell to follow [4]. In the absence of cAMP stimuli, un-polarized Dd cells extend pseudopods in random directions, presumably in order to determine a favorable direction in which to move. Polarized cells have a high propensity to extend new pseudopods on alternate sides at the leading edge, which facilitates maintenance of their direction of movement [5-7]. Aggregation-competent cells respond to cAMP stimuli with characteristic changes in their morphology. The first response is suppression of existing pseudopods and rounding up of the cell (the 'cringe response'), which occurs within about 20 s and lasts about 30 s [8,9]. Under uniform elevation of the ambient cAMP this is followed by extension of pseudopods in various directions, and an increase in the motility [10,11] and polarity [12,13]. A localized application of cAMP elicits the cringe response followed by a localized extension of a pseudopod near the point of application of the stimulus [14]. This type of stimulus is similar, although it varies more rapidly, to that a cell experiences in cAMP waves during aggregation. Cells undergo periodic shape changes from rounded to elongated in response to waves during aggregation [15], and waves elicit the cringe response [16]. Both polarized and un-polarized cells are able to detect and respond to shallow chemoattractant gradients of the order of a 2% concentration difference between the anterior and posterior of the cell [17]. While unpolarized cells are sensitive to directional cues at all points along the perimeter, polarized cells are more sensitive at their leading edge. Directional changes of a shallow gradient induces reorientation of polarized cells, whereas large changes

in the attractant lead to retraction of a pseudopod and formation of a new one in the direction of the stimulus [18, 19].

Cells also respond to static gradients of cAMP. Fisher et al. [20] showed that cells move faster up a cAMP gradient than down, and that the majority of turns made by a cell are spontaneous (although there is a reduction in the frequency of turns when the cell moves up the gradient). However, the magnitude and direction of a turn is strongly influenced by the gradient in that there is a strong tendency to move up the gradient. This was also demonstrated under treatment of latrunculin A (latA), where immobilized cells polarize their filamentous actin (F-actin) localization towards a directional cue [17]. Furthermore, aggregation is not affected by the absence of relay (treating cells with caffeine suppresses relay but does not impair their chemotactic ability [21, 22]).

In addition to responding to changes in cAMP, due for example to movement in a static gradient, local application of a stimulus, or the stimulus that results from cAMP waves in aggregation fields, cells also adapt to constant background levels of cAMP, which means that they respond to transient changes in the stimulus, but not to constant stimuli. This ability to adapt to the mean stimulation level over several orders of magnitude allows cells to respond to repeated stimulation's and develop sensitivity to small difference in the cAMP level across the cells [23, 24]. Detailed mathematical models based on the cAMP signal transduction pathway can reproduce this behavior [25, 26], and a cartoon model that illustrates the essential dynamics of excitation and adaptation is given in [2]. In any case, it should be noted that not all state variables return to pre-stimulus levels in systems that adapt – some state variables must change in order to compensate for changes in the background stimulus level [2].

The spatio-temporal chemotactic activities in *Dd* have been visualized by localization of tagged F-actin and other molecules within the chemotactic pathway, such as phosphatidylinositol-3,4,5-trisphosphate (PIP₃) and active Ras. The first phase of the response, which corresponds to 'cringing', is characterized by uniform and transient localization of these molecules along the cell periphery within 10 *s*. Then activity at the cell membrane drops after 30–50 *s* and is followed by the second phase of the response that involves localized membrane activity towards directional cues or in newly created pseudopods [27–29].

Many components in the signal transduction pathway governing chemotaxis in *Dd* have been identified. Ras is a family of small G-proteins whose two members, RasC and RasG, are the common regulators of parallel pathways that control chemotactic activities and are necessary for chemotaxis and relay of the cAMP signal in *Dd* [30]. They are also the most upstream molecules within the chemotactic pathway whose activity adapts [30, 31]. RasG is a primary regulator of phosphatidylinositol-3 kinase (PI3K), which converts phosphatidylinositol-4,5-diphosphate (PIP₂) into PIP₃, while RasC regulates activity of the target of rapamycin complex 2 (TORC2), a parallel pathway that regulates chemotaxis and signal relay. PIP₃ is a membrane lipid which contains a specific site that binds and activates many effectors containing a pleckstrin homology domain (PH domain). Its direct and indirect effectors include proteins such as RacB, RacC, and WASP that lead to F-actin polymerization, proteins such as PKB/Akt and PhdA that regulate cell polarity and chemotaxis, and the cytosolic regulator of adenylyl cyclase (CRAC), which is necessary for cAMP production. The PI3K activity is crucial for polarity, chemotaxis in a shallow gradient, and stimulus-dependent increase in motility and pseudopod generation [19, 32, 33]. Sasaki et al. [28, 34] showed that there is positive feedback between PI3K, F-actin, and Ras, and this feedback is

necessary for spontaneous generation of pseudopods in the absence of external stimuli. In fibroblasts, PI3K stabilizes membrane protrusions. Exogenous Rac activation drives creation of new pseudopods, but the activity is not sustained in the absence of PI3K activity [35].

Although the biochemistry underlying the Ras–PI3K–F-actin network has been well-studied, the mechanism leading to spontaneous pseudopod formation and robust biphasic responses to stimuli remains elusive. Early models addressed cAMP relay [25, 36] and spontaneous pseudopod formation [37]. More recently, a biochemical-based model [38] and an abstract model [39, 41] that exhibit the biphasic response have been proposed. The former was drawn from parametric optimization on an extensive signaling network where it is difficult to develop intuition and understand the underlying mechanisms. The latter provided an abstract model in which the signal adapts within an upstream network due to a feedforward mechanism. In this model detection of spatial gradients involves an activator-inhibitor mechanism [40], renamed as the local-excitation-global-inhibition (LEGI) network [39, 41], which is structurally similar to an earlier cAMP relay model [25]. However the LEGI model is formal, and no attempt has been made to identify the components with the known components of the signal transduction network. A recent study of Ras activity showed that adaptation occurs at this regulation step and argued that adaptation is due to feedforward control [24]. In addition, there are models that address polarization and spontaneous local PIP₃ activity, which may also be induced by external stimulation [42–44]. Jilkin and Edelstein-Keshet [45] give a more detailed account of existing directional sensing and polarization models, but despite extensive theoretical studies on the pathway, the roles of various molecular players in driving the processes that lead to robust and highly sensitive directional responses and cell polarity are not well understood. Further remarks on existing models are relegated to the discussion.

Here we propose a model based on known biochemistry that exhibits robust adaptation and amplification of extracellular signals, and for which the predictions match experimental observations. It consists of two modules: (i) an upstream module structurally similar to the biochemical model in [24] which regulates Ras activity by a feedforward control and is responsible for adaptation to the mean stimulus level and (ii) a downstream module which controls PIP₃ activity and amplifies subtle spatial gradients of Ras activity. In this model, detection of spatial gradients via the upstream module depends on the assumption that the characteristic decay length $L_d \equiv \sqrt{D_{(\cdot)}/k_{(\cdot)}}$, wherein (\cdot) denotes the species label, of RasGAP exceeds that of RasGEF. We later assume equal diffusion coefficients for RasGEF and RasGAP and the numerical values used for the decay constants lead to a ratio of $\sqrt{2}$ for the characteristic lengths. Thus this assumption is less restrictive than the assumption on diffusion coefficients needed in the LEGI framework, which requires the activator to be local and the inhibitor to diffuse rapidly [46]. Using this model, we study drivers for the first and second peaks of the actin response to stimulation, and the factors that control cell responsiveness to changes of the gradients and to the reapplication of uniform stimulation. We show that cell polarity regulates directional responses via cell geometry, and that the internal signal integrates with extracellular stimulation via the activity of RasGEF and RasGAP, the regulators of Ras. This unified framework exhibits dependence of polarization degree on the level of the stimulus, infers modes of migration, and explains directional persistence in polarized cells. Furthermore, it suggests positive feedback between cell shape and biochemical signaling that may lead to random pseudopodia extension and polarization, which is dependent on PI3K activity, and a potential role of cAMP secretion

in progressive development of cell polarity through the developmental cycle.

Biochemical pathways leading to PIP₃ responses

The first step in *Dictyostelium* chemotaxis involves binding of cAMP to CARs, G-protein coupled receptors (GPCRs) that transduce signals by activating heterotrimeric G proteins [47]. A cAMP-bound GPCR acts as a guanine nucleotide exchange factor (GEF) for the G_α subunit of the heterotrimeric G protein, causing dissociation of the activated G_α subunit and the G_{βγ} subunit. Hydrolysis of GTP in the G_α subunit induces re association, which diminishes active G-protein subunits when external cAMP is removed. Activation of the heterotrimeric G-proteins is enhanced by resistance to inhibitors of cholinesterase 8 (Ric8), a non-receptor independent GEF for G_α, which is specific to free G_α subunits [48]. Free G_{βγ}, of which there is only one type in *Dictyostelium*, is involved in activating the downstream PI3K chemotactic responses via RasGEF and ElmoE, as shown in Figure 1.

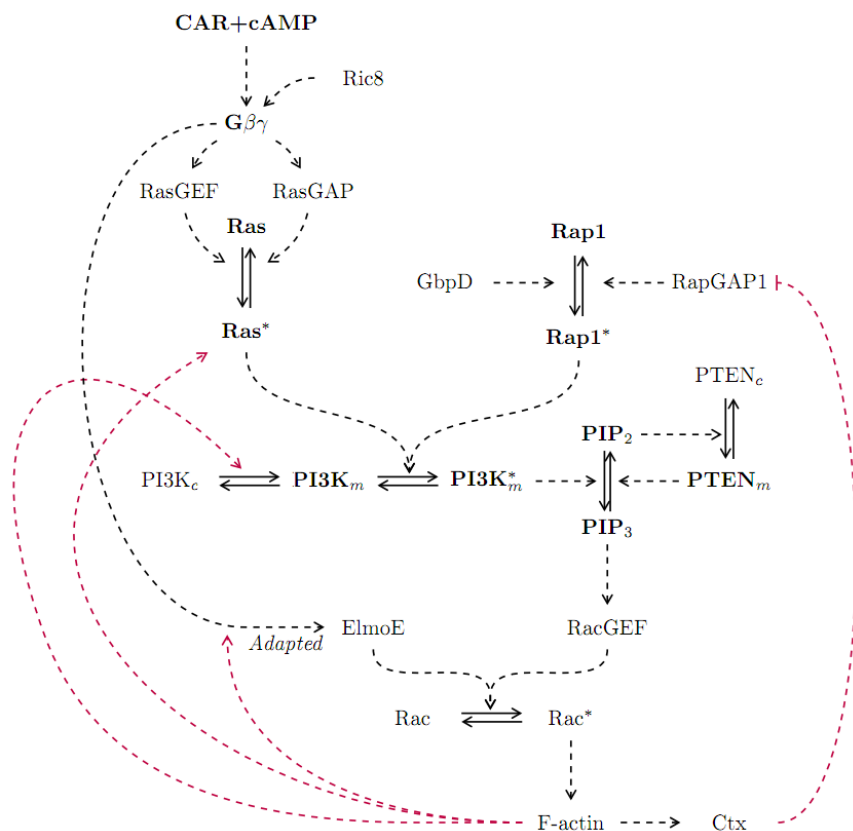


Figure 1. PI3K signaling pathway. Interconversion between different forms of the same molecule is denoted by solid arrows while positive regulation and promotion of a particular species and process are denoted by dashed arrows. Membrane-bound species are shown in bold while other species reside in the cytosol.

The first module in the network involves Ras, which acts as a molecular switch that cycles between an

active GTP-bound form and an inactive GDP-bound form. Conversion between the GTP and GDP-bound states is controlled by GTP exchange factors (GEFs), and GTPase activating proteins (GAPs). GEF proteins activate Ras by catalyzing the exchange of bound GDP with GTP, whereas GAPs inactivate Ras by increasing their rate of GTP hydrolysis. There are many GEFs in *Dictyostelium*, of which RasGEFA and RasGEFR, are involved in chemotaxis. GEFs are normally in the cytosol, but are recruited to the membrane in response to stimuli [49]. Active RasGEFA is responsible for activating RasC, while active RasGEFR is responsible for the majority of RasG activity [50]. RasC and RasG together are necessary for chemotactic responses at the leading edge and the trailing edge, as well as for cAMP secretion and cGMP production. RasC is necessary for the activity of the target of rapamycin complex 2 (TORC2) pathway, while RasG is uniformly distributed along the plasma membrane and directly activates PI3K [30, 51–53]. The only known RasGAP related to chemotaxis is DdNF1, which is partly responsible for RasG deactivation, and may be involved in detection of directed stimuli [31].

The activation of PI3K by active RasG depends on its localization at the membrane, and membrane localization of PI3K depends on F-actin activity [28, 51]. Active PI3K phosphorylates the membrane lipid PIP₂ into PIP₃ and the PI3K activity is balanced by phosphatase and tensin homolog (PTEN), which is recruited to the plasma membrane by PIP₂ and converts PIP₃ into PIP₂. Due to its specific PH domain, PIP₃ has many downstream effectors, including RacB and possibly RacC, and the activity of both Rac proteins ultimately leads to F-actin polymerization [54, 55]. In addition, RacB may be activated independently of the PI3K pathway via ElmoE, which is another effector downstream of G_{βγ} [56] (Figure 1). Although F-actin is still polarized by a cAMP gradient when PI3K activity is inhibited by LY294002, the PI3K activity is necessary for formation of random pseudopods and for the second peak of the F-actin activity under uniform cAMP stimulation. In fibroblasts, pseudopods formed by photo-activation of Rac are not stabilized in the absence of PI3K activity [27, 32, 34, 35, 57].

Many positive feedback steps have been identified in the PI3K pathway, including the actin-dependent localization of PI3K at the membrane. Moreover, unstimulated cells, as well as *gβ* null mutants, exhibit spontaneous localization of F-actin, PIP₃, PI3K, and Ras activity to regions of the cell membrane that coincide with pseudopod formation. Inhibition of either PI3K activity or F-actin leads to disruption of this spontaneous activity, although small pseudopodial projections are observed in the absence of PI3K activity. Interestingly, the local activity does not depend on the TORC2 pathway and substrate attachment. Moreover, disruption of RasG only leads to mild defects in the spontaneous activity [28, 34]. In addition, F-actin positively regulates Rap1, a Ras-subfamily protein that directly activates PI3K, via deactivation of RapGAP1. Ctx, an actin bundling protein, sequesters RapGAP1 and promotes Rap1 activity at the leading edge [58–60]. Studies have shown that the distribution of cAMP receptors remains uniform under stimulation, and localization of free G_{βγ} closely follows cAMP stimulation, suggesting that adaptation does not occur at this level [29, 61, 62]. Since Ras activity adapts to uniform stimuli while RasGEF remains active, adaptation of the chemotactic response probably occurs at this step. Membrane localization of ElmoE also adapts, and since its activity is independent of Ras activity, adaptation probably occurs here as well. From these observations it follows that the PI3K chemotactic pathway consists of a self-sustainable network of interconnected feedback loops whose inputs are upstream signals that adapt at the level of Ras and ElmoE.

To understand how the fundamental processes in the Ras and PI3K modules contribute to cellular response to stimuli, we first study a network that maintains key characteristics of the full pathway, namely, adapted input and positive feedback. We construct a model by selecting a minimal set of well-understood components of the network that is capable of producing the biphasic response that adapts to the mean stimulation level and amplifies spatial gradients of directional cues. The model includes the activity of RasGEF, RasGAP, Ras, PI3K, PTEN, and PIP₃, as shown in Figure 2. Because the heterotrimeric

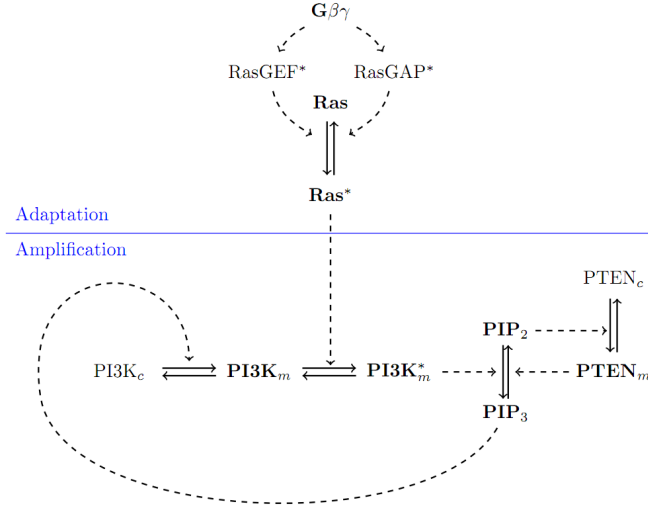


Figure 2. A simple model of the PI3K-signaling pathway. Membrane species are shown in bold.

G-protein activity closely reflects extracellular cAMP concentration at the membrane, we identify local membrane density of free $G_{\beta\gamma}$ as the input. Two-dimensional domains which represent cross sections of cells parallel to the substrate are employed for numerical simulations. As chemotactic responses in Dd are normally studied in latA-treated immobile cells which assume a circular cell shape, we first study the system on a 2D disk of $8 \mu m$ radius. Later we study the response to stimuli in more realistic cell shapes. A detailed description of the reactions involved and the evolution equations for the various species in the model is given in Methods section.

Results

Adaptation to uniform stimuli

As previously noted, Takeda et al. [24] suggested that adaptation in Ras activity is due to feedforward adaptation via activation and inactivation of Ras by RasGEF and RasGAP, both of which are activated by cAMP binding to CAR. They monitored Ras activation via membrane localization of Ras-binding domain (RBD), which diffuses freely in the cytosol and is localized to the membrane by binding to active Ras. We show the comparison between their observations and our model predictions in Figure 3, which shows the simulated bound RBD compared with the observations. The authors noted that the steady-

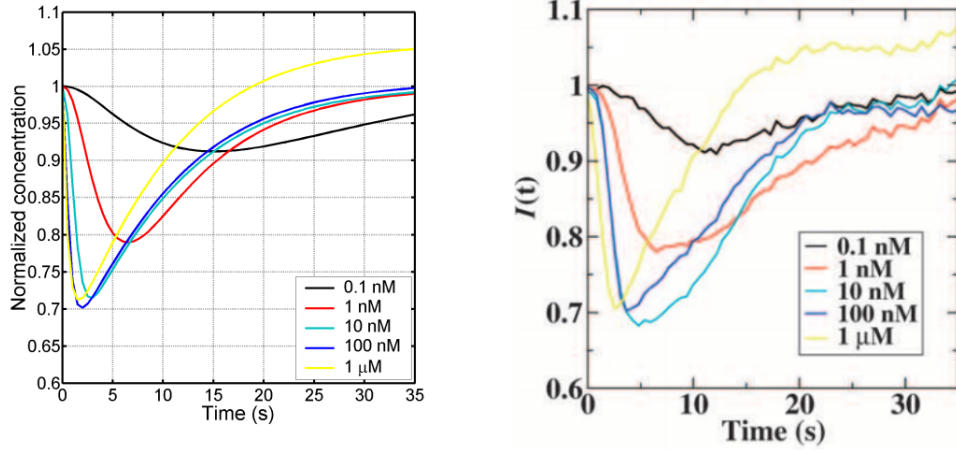


Figure 3. Ras-activation dynamics. Uniform stimulation causes a transient decrease in the average cytosolic concentration of RBD. The stimulus is applied at $t = 0$ s and response is measured over the physiological range of cAMP concentration. Simulation results (*left*) are compared to experimental measurements (*right*) from [24]. Here and hereafter simulation results are based on parameters in Table 1.

state Ras activity monitored drops below the basal level when the system becomes saturated at around $1 \mu\text{M}$ cAMP, and the figure shows that the model captures all aspects of the observed transient behavior, including more rapid adaptation at higher stimulus levels. Note that an undershoot of bound RBD – *i.e.*, a level below 1 – corresponds to an overshoot of the average cytosolic RBD shown in the figure. Our model, which is based on the measurements of cytosolic RBD intensity to determine rate constants given in Table 1 and used in the Ras module (Equations (1)–(7)), differs from those proposed earlier [24, 41] in that we allow both RasGEF and RasGAP to diffuse in the cytosol and maintain conservation of these proteins. It is precisely the conservation condition that leads to saturation of RasGEF and RasGAP activity at a high cAMP level.

Parameter	Value	Description	References
R	$8 \mu\text{m}$	Cell radius	
δ	10 nm	Effective length for membrane reactions	
$RasGEF_0$	$0.1 \mu\text{M}$	Average RasGEF cytosolic concentration	[88]
$RasGAP_0$	$0.1 \mu\text{M}$	Average RasGAP cytosolic concentration	[88]
Ras_0	$2000 \#/\mu\text{m}^2$	Membrane density of Ras	[38]
$PI3K_0$	$0.1 \mu\text{M}$	Average PI3K cytosolic concentration	[88]
$PTEN_0$	$0.1 \mu\text{M}$	Average PTEN cytosolic concentration	[88]
PIP_0	$1000 \#/\mu\text{m}^2$	Membrane density of PIP_2 and PIP_3	[42, 88]
D_{RasGEF}	$10 \mu\text{m}^2/\text{s}$	Diffusion constant for RasGEF	[89]
D_{RasGAP}	$10 \mu\text{m}^2/\text{s}$	Diffusion constant for RasGAP	[89]
D_{PI3K}	$10 \mu\text{m}^2/\text{s}$	Diffusion constant for PI3K	[89]
D_{PTEN}	$10 \mu\text{m}^2/\text{s}$	Diffusion constant for PTEN	[89]
k_{RasGEF^*}	$93.75 (\#/\mu\text{m}^2)^{-1} \mu\text{m}/\text{s}$	RasGEF activation by $G\beta\gamma$	
k_{RasGEF}	0.25 s^{-1}	Spontaneous RasGEF* deactivation	

Parameter	Value	Description	References
k_{RasGAP^*}	$1.5 (\#/\mu m^2)^{-1} \mu m/s$	RasGAP activation by $G\beta\gamma$	
k_{RasGAP}	$0.12 s^{-1}$	Spontaneous RasGAP* deactivation	
k_{Ras^*}	$800 \mu M^{-1} s^{-1}$	Ras activation by RasGEF*	
k_{Ras}	$2.5 \times 10^6 \mu M^{-1} s^{-1}$	Ras* deactivation by RasGAP*	
k_{s,Ras^*}	$3.14 \times 10^{-4} s^{-1}$	Spontaneous Ras activation	
$k_{s,Ras}$	$0.03 s^{-1}$	Spontaneous Ras* deactivation	
$k_{PI3k_m^*}$	$18.75 (\#/\mu m^2)^{-1} s^{-1}$	PI3K activation by Ras*	
$k_{d,PI3k_m}$	$0.844 s^{-1}$	Spontaneous PI3K* deactivation	
k_{PI3k_c}	$3 \times 10^5 s^{-1}$	Spontaneous PI3K membrane dissociation	
k_{PI3k_m}	$1500 \mu M^{-1} s^{-1}$	PI3K membrane binding induced by PIP ₃	
k_{PIP_3}	$720 (\#/\mu m^2)^{-1} s^{-1}$	PIP ₃ production by PI3K	
k_{PIP_2}	$1050 (\#/\mu m^2)^{-1} s^{-1}$	PIP ₃ dephosphorylation by PTEN	
$k_{b,PI3k_m}$	$1500 s^{-1}$	Spontaneous PI3K membrane binding	
k_{PTEN_m}	$0.75 \mu M^{-1} s^{-1}$	PI3K membrane binding induced by PIP ₂	
k_{PTEN_c}	$0.375 s^{-1}$	Spontaneous PTEN membrane dissociation	

Table 1. Parameter values used in the model of the PI3K-signaling pathway.

In more detail, the transient decrease in cytosolic RBD observed experimentally corresponds to an increase in Ras activity, which is due to faster activation of RasGEF than RasGAP. Further, notice that the peak of Ras activity increases, whereas the activation time and the adaptation time decrease with increases in the cAMP level up to $\sim 10 nM$. The model predicts a similar trend in the response times, and shows that the rates of Ras activation and inactivation by RasGEF and RasGAP are strongly stimulus dependent. Moreover, return to the basal Ras activity in the model is ensured when both RasGEF and RasGAP activity is unsaturated, for then their steady-state activities are proportional, which renders the steady-state Ras activity independent of stimulation, provided spontaneous Ras activation and deactivation are negligible. Saturation of RasGEF and RasGAP leads to under- and over-activation of Ras at the steady state. In the simulation, RasGEF becomes saturated before RasGAP, resulting in a lower Ras activity and more free RBD.

Detection of spatial gradients by PI3K-PIP₃ feedback loop

To determine how well the model predicts the response to directional cues, we compare the predictions with the measured PIP₃ activity at the front and the back of an immobilized latA-treated cell reported in [29]. There the cell was subject to cAMP application from a micropipette and exhibited a biphasic response as shown in Figure 4. We simulated the experimental stimulation by a step change in cAMP concentration from a uniform basal level to a static spatial gradient with a mean level of $100 nM$, which simplifies the spatio-temporal profile of cAMP experienced by the cell. In reality cAMP reaches the leading edge faster the trailing edge, as shown in [26]. The step stimulation is applied to a circular cell whose upstream Ras module was described earlier and downstream network comprises the PI3K-PIP₃

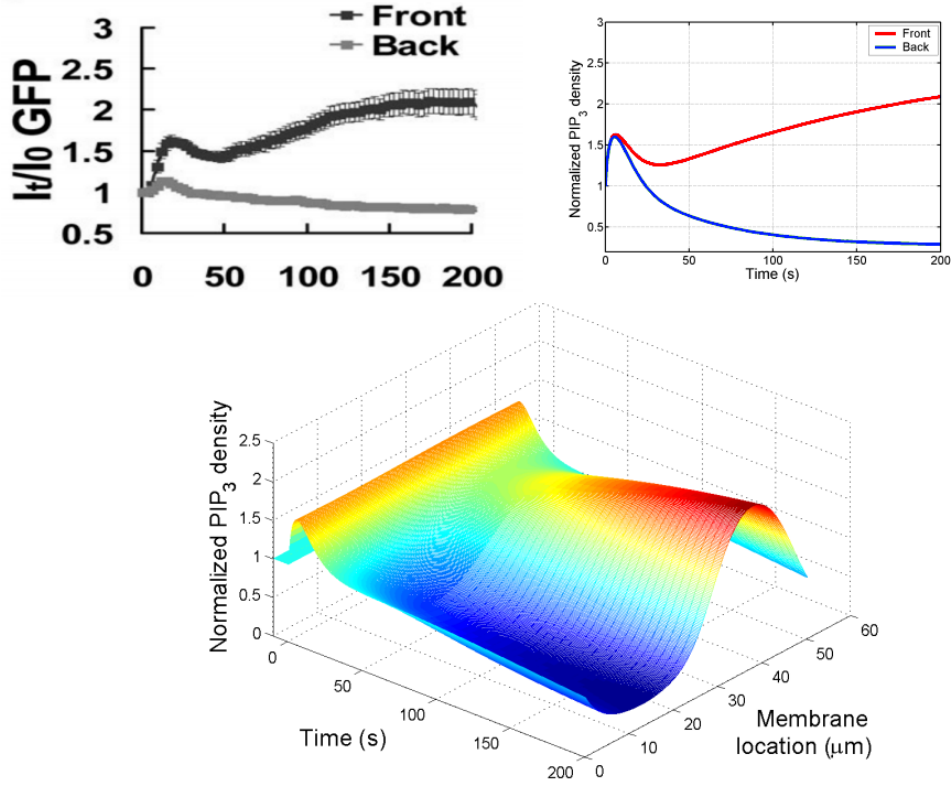


Figure 4. PIP₃ responses to a static cAMP gradient. (*Upper left*) The response at the front and the back of a cell to a cAMP gradient created by a micropipette. The cell is treated with latA and assumes a circular shape while the responses are measured by the local PH_{Crac}-GFP concentration [29]. (*Upper right*) The simulated PIP₃ response on a circular domain subject to a cAMP gradient with 50 % front-to-back difference. (*Lower*) Dynamics of the PIP₃ response along the cell membrane, starting and ending at a location with the mean cAMP level. The static gradient is applied to a resting cell at 0 s.

amplification module shown in Figure 2 (Equations (8)–(15)).

Under a directional cue, the localization of steady-state Ras activity is determined by the ratio between the local activities of RasGEF and RasGAP on the membrane. Degradation of active RasGEF and RasGAP, which are activated at the membrane, is characterized by the characteristic decay length $L_d = \sqrt{D/k}$ defined earlier. Differences in the L_d of active RasGEF and RasGAP leads to differences in their spatial profiles and results in localization of Ras activity. In particular, when $L_{d,RasGAP} > L_{d,RasGEF}$, RasGAP is more evenly distributed than RasGEF in the cytosol, with its level lower than that of RasGEF at the front and higher at the rear. This establishes a steady-state gradient of Ras activity that follows the directional cue. On the other hand, if $L_{d,RasGAP} < L_{d,RasGEF}$ the gradient is reversed. If the diffusion of RasGAP is large compared with that of RasGEF then RasGAP is essentially spatially uniform, and in this case the ratio between Ras activity at the anterior and the posterior, normalized by the ratio in cAMP levels approaches 1.

The PI3K-PIP₃ amplification module combines positive feedback via membrane recruitment of PI3K

and cooperativity due to separate PI3K recruitment and activation steps, and is capable of significantly amplifying the weakly localized Ras activity, which is shown in [63]. Parameters for the PI3K-PIP₃ subnetwork are obtained by matching the dynamics of PIP₃ response at the front and the back of the cell with an observation in [29], where a 20 % cAMP gradient across the cell diameter induces ~180% change in the PIP₃ gradient. Figure 4 displays the PIP₃ dynamics around the membrane of a cell that experiences ~50% front-to-back difference in cAMP concentration, and compares the numerical simulation to the experimentally-observed PIP₃ activity of a cell subject to cAMP released from a micropipette.

The response displays the distinctive biphasic behavior characteristic of a cringe, which occurs in response to directional cues as well as uniform stimuli. Upon stimulation, PIP₃ density over the entire cell membrane increases rapidly, reaching the first peak within 10 s. Then the PIP₃ density drops throughout the membrane before it starts to rise selectively at membrane locations above the mean of the cAMP gradient after ~50 s, which establishes cell orientation. The first peak is due to the transient Ras activity that adapts to the mean cAMP level, as the PIP₃ response does not exhibit the transient peak in response to stimulation with a constant mean cAMP level. On the other hand, the spatial sensitivity displayed by steady-state PIP₃ localization at the leading and trailing edges is due to significant amplification of small differences in local Ras activity by the PI3K-PIP₃ subnetwork. This process is slower than activation and adaptation to the new cAMP level, thereby producing a distinctive drop in PIP₃ level before the separation between the front and the back sets in. Notice that the observed first peak at the trailing edge is lower than the peak at the leading edge while the simulated response exhibits almost identical peaks. This could be due to delayed exposure to cAMP experienced by the trailing edge [26], which was omitted in the simulation.

Uniform stimulation with repeated increases in cAMP concentration produces adapting PIP₃ responses that are identical in the front and the back of the cell, as shown in Figure 5. The combined

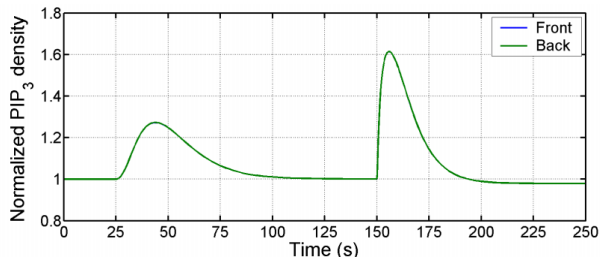


Figure 5. PIP₃ response to repeated stimulation. PIP₃ localization at two opposite points on the membrane of a circular cell subjected to successive steps of spatially uniform stimulation. The stimulation is represented by the local level of free $G_{\beta\gamma}$ which reflects 0.1 nM and 100 nM cAMP at 25 s and 150 s respectively. The responses at the two sites are nearly identical.

adaptation-amplification mechanism allows consistent localization of PIP₃ activity over several orders of magnitude in mean cAMP concentration. Thus this direction-sensing model can be used to study reorientation, polarization, and the roles of PI3K in motility and spontaneous activity in Dd cells. Note that in our simplified model shown in Figure 2 the experimentally-observed positive feedback from F-actin to Ras activation has been omitted, allowing independent analysis of the effects of ‘upstream’ Ras activation

and ‘downstream’ PIP₃ activity. One can include positive feedback to Ras so that its activity is sensitive to spatial gradients, while maintaining adaptation to the mean cAMP level, and this will be discussed later.

It is known that Dd cells are able to reorient themselves when a cAMP gradient is reversed. Meier et al. [16] observed that the ability to reorient is limited by polarization dynamics, and *Dictyostelium* cells become trapped under stimulus gradients with rapidly changing direction. Chemotaxing cells move up the cAMP gradient with reduced speed when subjected to alternating cAMP gradients with a period of 120 s compared to 600 s. They are completely stalled and trapped within the alternating gradient when the period is 20 s. Figure 6 displays simulations of PIP₃ dynamics under alternating gradients at 20 % difference with periods of 20, 120, and 300 seconds, which agree well with the experimental observations. The response develops a very small front-to-back gradient at the highest frequency, which explains its

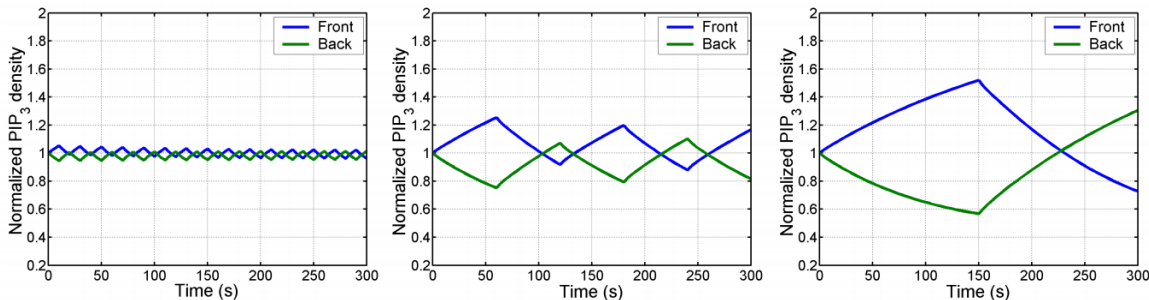


Figure 6. PIP₃ responses to alternating gradients of different periods. (Left) 5 s, (middle) 120 s, and (right) 300 s.

inability to polarize under the rapidly-alternating gradient. As the frequency decreases, stronger PIP₃ localization gradients are allowed, leading to the experimentally-observed increase in the chemotaxis speed.

The roles of cellular shapes in polarization and motility

Polarized cells are elongated and have a well-defined anterior and posterior. In the absence of directional stimulation, they move persistently in the direction of their anterior and only change direction significantly every 9 minutes on average. They migrate by alternately splitting left and right pseudopods from their leading edge, between 40° and 70° to their polarization axis, and occasionally develop *de novo* pseudopods which cause abrupt changes in the movement direction [6, 7, 19]. Experimental observations suggest that the polarization of Dd and neutrophils depends on PI3K activity and that these cells become more polarized at higher levels of persistent uniform stimulation [5, 64–66]. To study the PI3K activity in polarized cells, we apply various types of cAMP stimulation to 2D simulation domains which resemble the shape of polarized cells on the substrate surface. Since shape changes are slower than biochemical re-polarization, we study the chemotactic responses in frozen domains as a first step to approximate the dynamics of signaling proteins in motile cells. Recent work [67] on the network downstream of PIP₃ that leads to F-actin polymerization will be discussed later.

Our simulation results suggest that biochemical polarization is at least partly determined by the spatial configuration of the cell, particularly the curvature of the membrane. Figure 7 depicts the steady-state PIP₃ localization of polarized cells subject to uniform stimulation. PIP₃ is localized strongly at

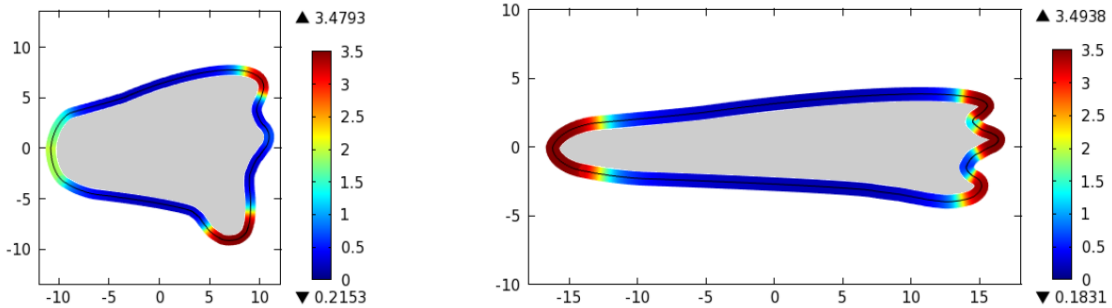


Figure 7. The steady-state PIP₃ localization at the boundary of cells subject to uniform stimulation at 100 nM cAMP. (Left) A moderately polarized cell. (Right) A highly polarized cell. Reaction-diffusion equations are solved in the regions shown. Color bars display PIP₃ activity at the boundary, normalized by its unstimulated level. Boundary curve is inflated to show color variations.

the left and right protrusions at the leading edge of the moderately polarized cell, with stronger PIP₃ localization in the right pseudopod, in good agreement with observations which show that pseudopod extension occurs at the left and the right of the leading edge [7]. On the other hand, PIP₃ is strongly localized at all anterior protrusions in the strongly polarized cell, suggesting a more unimodal distribution in the direction of pseudopod extension. Interestingly, PIP₃ is also localized, moderately and strongly, at the trailing edge of the moderately and strongly polarized cells, respectively. Simulated PIP₃ localization in cells polarized in the direction of increasing cAMP is consistent with observed localization of many signaling molecules within the pathway, including F-actin, PI3K, PIP₃, and RacB, in cells migrating towards directional cues [31,54,68]. Figure 8 compares the simulated PIP₃ localization to the experimental observations.

Simulated PIP₃ activity influenced by the cell shape tends to localize in re-entrant regions of the boundary, such as tips or narrow tethers, in good agreement with measurement of PIP₃ localization in fibroblasts [69]. Examination of Ras activity, which exhibits subtle localization under uniform stimulation, suggests that the pronounced PIP₃ localization is due to amplification of the active Ras spatial profile. Figure 9 displays the spatial localization of RasGEF and RasGAP activities and their ratio at the steady state. Both activated RasGEF and activated RasGAP are localized in re-entrant regions, but activated RasGAP is more uniformly distributed. Their ratio at the boundary, which determines the Ras activity at the membrane, is also higher in these regions than elsewhere. To rationalize the PIP₃ localization caused by Ras activity, which is in turn regulated by active RasGEF and RasGAP, we sought to understand how the cell shape affects localization of RasGEF and RasGAP activities under uniform stimulation. We analyzed the steady-state activation profiles of a membrane-activated molecule in a 3D shell and a thin strip to better understand the effect of the mean curvature of the domain and the distance between boundaries, respectively, on localization. These cartoon descriptions allow for analytical solutions (see

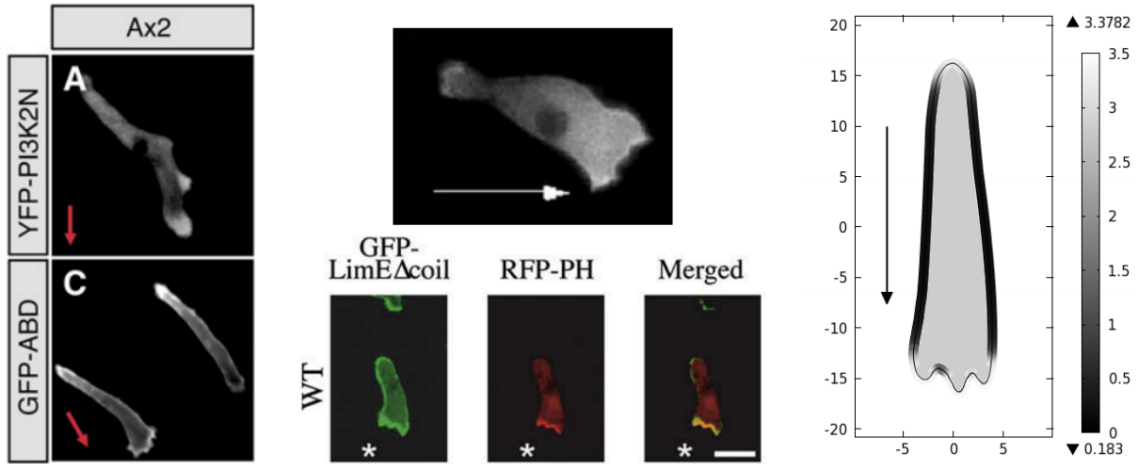


Figure 8. Localization of signaling molecules in highly polarized cells migrating towards cAMP sources. The directions of cAMP gradients are indicated by arrows. Stars indicate tips of micropipettes. (*Left panel*) PI3K localization (*top*) and F-actin activity (*bottom*) are the highest at the posterior and at protrusions and membrane ruffles near the anterior [68]. (*Middle panel, top*) RacB activity, which is downstream of PIP₃ is high at the front and noticeable at the back of the cell [54]. (*Middle panel, bottom*) F-actin (*green*) and PIP₃ (*red*) activities are highest near the micropipette. The activity at the back of the cell is also above the normal level [31]. (*Right panel*) Simulated PIP₃ activity under a 50 % front-to-back gradient is the highest at the anterior. There is also significant PIP₃ activity at the posterior.

the Methods section) which are plotted in Figure 10.

In the case of the 3D shell, the difference in curvature contributes to the difference in the activity at the inner and outer membrane, where the convex (viewed from the interior of the shell) outer membrane is less exposed to the bulk cytosol than the concave inner membrane, leading to higher activity at the outer membrane. The ratio between the outer and inner activity depends on the difference in curvature and the distance between the inner and outer membrane. For an infinite strip, the membrane activity decreases as the strip becomes wider because the activity at one boundary has less effect on the other side. It approaches a constant when a molecule activated at one side fails to reach the other side before it becomes inactive. If we subtract the asymptotic (in the width) amplitude from the result in the lower right, and fit the remainder with an exponential, the decay constant in membrane activity as a function of the domain width approximately coincides with L_d . In summary, we found that membrane along a thin region may have much higher activity than membrane within the same cell that is well exposed to cytosol, and that membrane curvature contributes to its cytosolic exposure. Moreover, an exposed membrane region may also have high activity if it is in close proximity to a region with high activity. Ras and PIP₃ localization follows the localization of active RasGEF and RasGAP, since $L_{d,RasGAP} > L_{d,RasGEF}$, and small variations in RasGEF and RasGAP activity may ultimately lead to highly-polarized PIP₃ activity due to amplification by the PI3K-PIP₃ subnetwork. Thus when a cell is subjected to a directional cue, the spatial distributions of active RasGEF and RasGAP are dictated by both cell shape and stimulation, in effect integrating the intrinsic polarity with the external information to produce

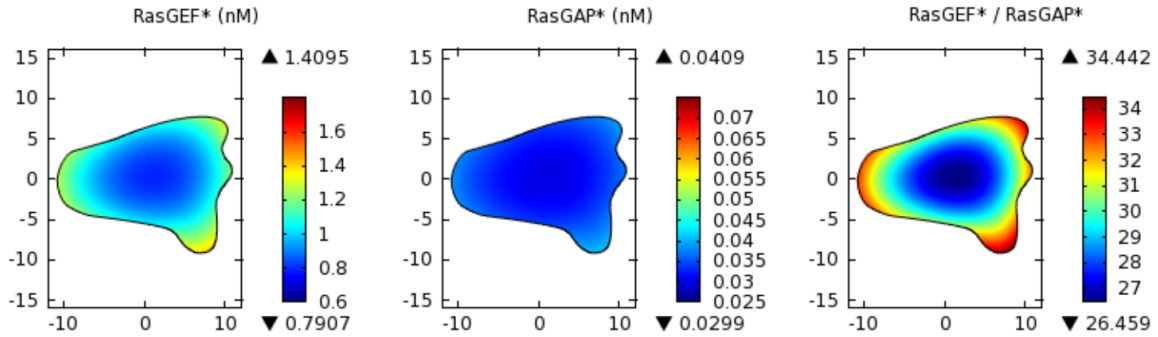


Figure 9. The steady-state activities of RasGEF and RasGAP under uniform stimulation.

‘biased’ PIP₃ polarization. This intrinsic polarity that derives from the cell shape is in contrast to explicit polarity studied in [70, 71].

The shape-induced polarization of PIP₃ is dependent on the mean cAMP level, as shown in Figure 11 for spatially-uniform stimulation at various cAMP levels. The dependence arises from the balance between spontaneous GTP hydrolysis and turnover of Ras and cAMP-dependent RasGEF and RasGAP activities, which are affected by cell shape. One can see that the degree of polarization is an increasing function of the stimulus level except at 1 μ M, where RasGEF begins to saturate (*cf.* Figure 3). Wang et al. [72] observed that removal of the stimulus leads to a transient decrease in the PIP₃ level, which is consistent with the recovery time of approximately 3 minutes that is required before fully-adapted Dd cells become responsive to new stimulation at the previous cAMP level [62, 72, 73]. While a simple feedforward control leads to slow recovery after cAMP removal, which depends on the cAMP level, the modulation between spontaneous and cAMP-induced regulation of Ras ensures the recovery period for the signaling pathway is consistent with *in vivo* observations. Note that although PIP₃ activity is high at many locations along the cell membrane, total PIP₃ activity may drop slightly compared with the pre-stimulation level because saturation causes lower average activity within the cell, as observed *in vivo* [27]. Figure 12 displays average PIP₃ dynamics within 180 s after uniform stimulation.

In the absence of directional cues, polarized cells migrate persistently in the direction of their polarity. Our model suggests that there is positive feedback between cell polarity encoded by the cell shape and intracellular signaling that leads to F-actin localization and promotes pseudopod extension. Small protrusions at the anterior induce localization of PIP₃ and F-actin, which in turn drive the extension, contributing to directional persistence. Moreover, in moderately polarized cells, PIP₃ tends to localize within the protrusion at the left and right ends of the anterior, where membrane length per cytosolic area is the highest. This selective localization leads to high propensity of extending new pseudopods at an angle to the polarization axis. If there is a slow negative feedback to the F-actin localization process, due for example to scarcity of Arp2/3 and G-actin, as described in [67, 74] that causes retraction of older pseudopods, the overall process could result in the characteristic zig-zag movement observed *in vivo* [6, 7, 19].

When subject to a directional cue, RasGEF and RasGAP activity is determined by both the cAMP

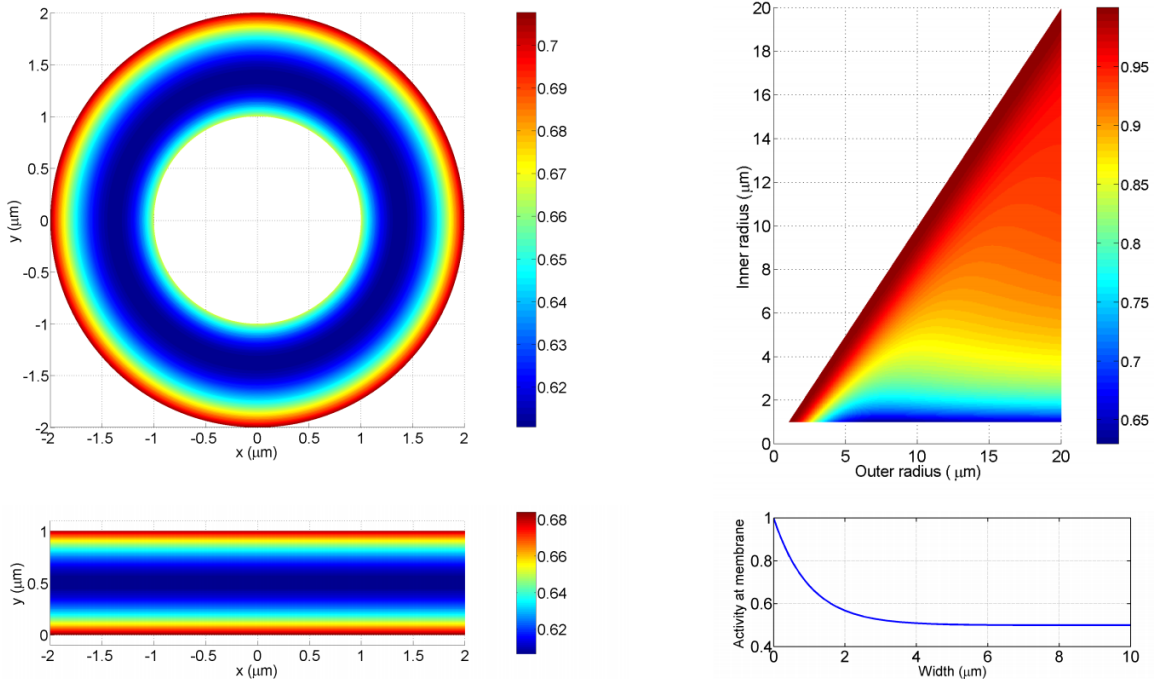


Figure 10. The steady-state activity of a membrane-activated protein in a cross section through the center of a 3D shell (*upper*) and an infinite strip (*lower*). (*Right column, upper*) The ratio between the protein activity at the inner and outer radii of shells with various sizes. (*Right column, lower*) The protein activity at the boundary of infinite strips of various width. In these simulations, $L_a = L_d = 1 \mu m$, where the characteristic lengths L are defined in the Methods section.

gradient and shape-induced polarity. Unlike a rounded latA-treated cell, which reorients its PIP₃ localization directly upwards a cAMP gradient, a polarized cell exhibits PIP₃ localization that is influenced by both factors. Usually, polarized cells maintain their polarity and make gradual turns towards the cAMP source and reorient themselves only when they are subjected to a strong cAMP gradient [5, 19, 27]. We can determine the chemotactic responses in polarized cells predicted by the model by applying cAMP gradients at different levels and directions. Figure 13 displays the steady-state PIP₃ localization biased by the gradients. Under uniform stimulation, the PIP₃ localization is the highest at the right pseudopod. Figure S1 depicts the localization dynamics. A 50%-gradient towards the top induces a clear directional bias for the left pseudopod. A 20% backward gradient cannot overcome intrinsic polarity and the PIP₃ localization at the right pseudopod remains the strongest. At steeper gradients, PIP₃ localization directly orients towards the back of the cell. Taken together, the numerical results suggest that a directional gradient normal to the polarity axis induces a turn towards the cAMP source by extending a pseudopod from the anterior at the position closest to the source. The cell gradually turns around maintaining its anterior and posterior under a shallow gradient that directs backwards while it reorganizes a new anterior directly at the back when subject to a strong backward gradient. Figure S2 shows PIP₃ localization dynamics corresponding to Figure 13b. In the first phase, PIP₃ localization peaks throughout the membrane due

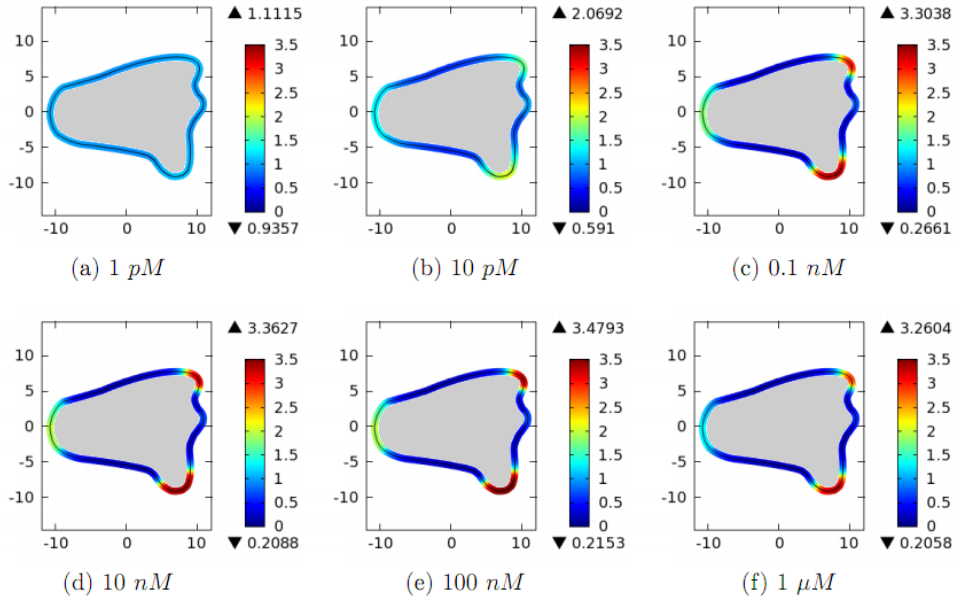


Figure 11. The steady-state PIP_3 localization in a moderately polarized cell at different levels of uniform stimulation.

to adaptation to the mean cAMP level. Then the PIP_3 level drops and selectively localizes at the top of the leading edge, implying the cell will continue migrating forward, with an upward bias.

An interesting experiment by Houk et al. [75] suggests that membrane tension, and not protein regulation, plays the role of global inhibitor for local protrusion. In this experiment, cells were subject to a heat shock, causing them to assume an irregular shape where the front and the back were separated by a long and narrow tether. Under the hypotheses of the biochemical model, activator and inhibitor would have been trapped in the front and the back respectively, the back should not have been able to resume spontaneous protrusion. However, after the tether is severed, the former back resumes spontaneous pseudopod extension, suggesting that the inhibition is not biochemical. We investigate if our signal transduction model is able to explain this interesting behavior. In our simulations, less than 20% of PI3K and PTEN is bound to the membrane while total concentration of RasGEF and RasGAP is uniform in the cytosol. Therefore, by separating the front and the back, only the concentration of PI3K and PTEN will change. According to our model, the change in PI3K and PTEN density alter the sensitivity curve for PIP_3 localization. The former front will generally have more PIP_3 activity while the former back will have less PIP_3 activity. Nevertheless, both halves are still capable of forming spontaneous protrusions. In fact, this agrees well with the observations in [75] as the former front undergoes excessive protrusions after it becomes free. Note that while the cell assumes the tethered shape, membrane tension could indeed play a major role in restricting protrusions within the tether and the back.

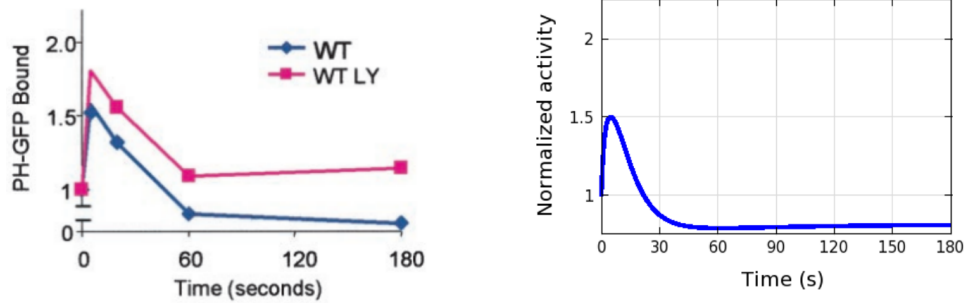


Figure 12. Dynamics of overall PIP_3 responses in wild-type cells. Uniform stimulation with $1 \mu\text{M}$ cAMP is applied at 0 s. (Left) Experimental measurement in wild-type (WT) and LY294002-treated cells [27]. (Right) Simulation of the moderately polarized cell.

Discussion

We developed a modular model for the network involved in signal transduction and the first steps in control of the actin network in eukaryotic cells. The model incorporates biochemical interactions that are well-established in *Dictyostelium* and captures many aspects of its responses to cAMP stimulation. The model consists of adaptation and amplification modules that are responsible for regulation of Ras and PIP_3 activities, respectively. Simulations of this model give insights into dependence of cell polarization on mean stimulus levels, how it is embedded in cell shapes, how it influences pseudopod extension and creates zig-zag movement pattern, and how it integrates with directional signals and gives directional persistence.

The adaptation module leads to rapid excitation and slower adaptation of Ras activity by feedforward regulation of its activator (RasGEF) and its inhibitor (RasGAP) over the relevant range of cAMP stimuli. Although it is unclear how RasGAP is activated by the external stimulus, the feedforward regulation is a simple scheme which serves well for adaptation of a molecular switch like Ras. Ras activity is able to adapt to repeated uniform stimulation, and the extent of adaptability is determined by saturation of either RasGEF or RasGAP activity. Recently-observed over-adaptation of Ras activity at high cAMP levels indicates that the inhibition signal is not downstream of Ras, and supports a control scheme such as we use, in which RasGEF activity is saturated before RasGAP activity [24]. Over-adaptation serves a useful purpose in that it serves to prevent elevated F-actin activity at saturating cAMP levels. When a stimulus is removed, there is an under-shoot of the Ras activity [39], and a recovery period is required before the cell becomes fully active to the previous stimulation level. This recovery time is dependent on the spontaneous GTP hydrolysis activity of Ras.

We found that the observed transient peak in F-actin shortly after the stimulus is applied is largely due to the adaptation mechanism, while the second, less-pronounced, phase of the chemotactic activity is due to amplification of small spatial variations of Ras activity along the membrane. In the feedforward model, the transient peak in Ras activity is caused by fast activation of RasGEF and slow activation of RasGAP. In the presence of a cAMP gradient, the assumption that RasGAP has a longer decay length than RasGEF leads to a stable gradient in Ras activity that mirrors the cAMP gradient. Our model

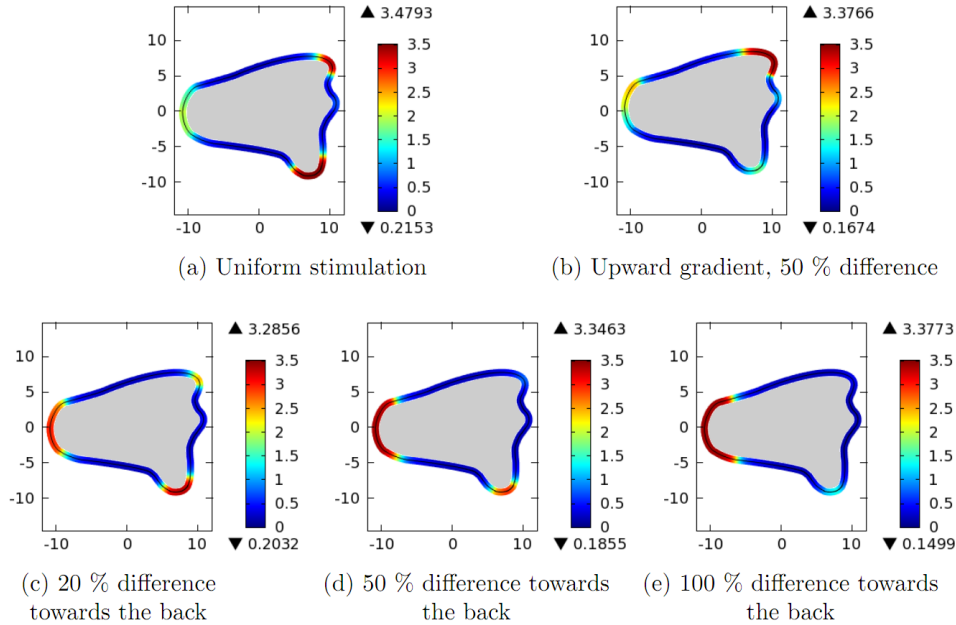


Figure 13. The steady-state PIP_3 localization of a polarized cell induced by static cAMP gradients. (a) A polarized cell subjected to uniform stimulation displays highest PIP_3 localization at the lower pseudopod. (b) A 50% cAMP gradient across the cell, along the y -axis, biases the localization towards the upper pseudopod. (Lower row) PIP_3 localization subject to backward cAMP gradient, along the negative x -axis, at different levels suggests distinct modes of movement. (c) biased movement induced by 20% gradient across the cell. (d) and (e) The cell reorients its front under large cAMP gradients.

differs from the activator-inhibitor type in that we do not assume that RasGEF diffuses much more rapidly than RasGAP – in fact they have equal diffusion coefficients in our simulations.

The amplification module involves the regulation of PIP_3 by PI3K and PTEN, and positive feedback that is sensitive to latA (which suggests dependence on F-actin). The activity of PI3K depends on both its membrane localization due to the F-actin activity and subsequent activation by Ras [32]. This two-stage activation of PI3K is sufficient to induce a greatly-amplified spatial gradient of PIP_3 activity without the usual assumptions of cooperative binding. Analysis shows that this network structure allows a sigmoidal response with arbitrarily high amplification [63]. Therefore small variations in Ras activity can be amplified into significant PIP_3 gradients along the membrane, thereby ensuring a suitable directional response. The biphasic response is a result of distinct time scales for adaptation and the PIP_3 dynamics, which becomes apparent after ~ 50 s and takes several minutes to fully develop. The time scale for developing PIP_3 orientation coincides with the ability of *Dictyostelium* to reorient and migrate under rapidly alternating cAMP gradients, suggesting an important role for PIP_3 activity in cell orientation [16].

In this work we incorporated only the structure necessary to produce the observed responses, and have omitted positive feedback that affects Ras activity and causes localization of RBD to spontaneously-extended pseudopodia [34]. In fact, this second positive feedback loop (see Figure 1) is also needed to

produce significant Ras localization under directional stimulation. If Ras activation via this positive feedback loop acts independently of activation by the external stimulus, for example by independent sites on Ras, adaptation will be preserved under suitable conditions on the feedback. In this case, any activity of PIP₃ and F-actin that occurs spontaneously will be observed in Ras as well. An analysis of adaptation with positive feedback from F-actin under the foregoing condition is given in the Methods section, and more detailed descriptions of the pathway are the subject of future work. Although this work is focused on the Ras–PI3K interaction (see Figure 2), there may be other inputs for the PI3K pathway such as Rac activation via ElmoE. Each input may trigger the feedback network shown in Figure 1 and cause directed migration. For example, photoactivation of Rac can direct neutrophil migration and it was demonstrated that PI3K is critical to this activity. [76]

We have shown that asymmetric cell shapes can lead to spatially non-uniform Ras activity, which is then amplified into PIP₃ gradients. In this case, PIP₃ localization is determined by a combination of chemotactic and geometric factors, the latter of which can be considered an intrinsic polarization of the cells. In narrow regions of a cell, activated RasGEF is more localized near the boundary than activated RasGAP, causing higher than average local Ras activity. This integration of cell polarity with localization of PIP₃ and its effectors suggests a role for membrane ruffles within the cell anterior in maintaining polarity of the cells. Similarly, filopodia may serve as precursors for pseudopodia. Moreover, because PIP₃ tends to localize more strongly in regions where the membrane curvature is large, this may cause polarized cells to preferentially extend pseudopodia at a large angle to the polarization axis if small regions of high curvature develop there. If these extensions in a hypothetical cell are out of phase, the cell could alternately extend pseudopod branches and display the zig-zag migration pattern observed in *Dictyostelium* chemokinesis [6, 7]. In contrast, more polarized cells without ruffles or other local small protrusions have PIP₃ concentrated throughout the leading edge, and will migrate more directly toward the stimulus. Because PIP₃ localization amplifies the Ras distribution, which is a combination of intrinsic polarity and external stimulation, the balance between them determines modes of directed migration. In a shallow cAMP gradient, polarized cells turn towards the stimulus source slowly, while maintaining their leading edge. On the other hand, when the directional cue overcomes the bias, PIP₃ is most strongly oriented towards the source, causing the cells to develop new anterior in this direction.

Neutrophils and starved *Dictyostelium* cells become more polarized and have increased motility under uniform stimulation [12, 13, 65]. These behaviors are dependent on PI3K activity [32, 33, 66], and our model suggests that such activity can be a result of modulation between small spontaneous self-activation and actively-regulated Ras activity, and that the polarity of the PIP₃ signal is dependent on the cell conformation, creating a positive feedback between biochemical and physical attributes of the cell. The implications of this are two-fold. Firstly, this positive feedback could potentially lead to spontaneous pseudopodia extension. The onset of spontaneous protrusions could be the result of F-actin waves, which perturb membrane conformation. In fact, observations in *Dictyostelium*, neutrophils, and fibroblasts suggest that pseudopod extension frequency is dependent on the stimulation through the PI3K pathway and that breaking the feedback loop by PI3K inhibition disrupts the ability to sustain polarity, even when local protrusions are induced by photo-activation of Rac, which is downstream of PIP₃ [35, 65, 76]. Secondly, the fact that polarization of *Dictyostelium* is dependent on the external cAMP level may link

polarity to signal relay in starved *Dictyostelium* cells, where secretion of cAMP serves as a means to develop self-induced polarity [13].

In this work, we elucidated how the cell shape and intracellular signaling are related to cell motility and polarization. In future work, we will incorporate cell movement into the current model to better understand the interplay between signaling and the cell shape and how this determines extension and survival of pseudopods. Spontaneous actin waves associated with PI3K activity as well as spontaneous PIP₃-PTEN dynamics have been observed in *Dictyostelium* and could play roles in driving spontaneous pseudopod extensions and retractions [77, 78]. Our signaling model incorporates neither the positive feedback through Ras nor the cooperativity within the PI3K feedback loop due to branching of F-actin and is not excitable, despite exhibiting high gradient amplification. We have studied the actin waves using a model which incorporates F-actin branching [67] while PI3K-based models which include cooperativity have been proposed to study the PIP₃-PTEN dynamics [78, 79]. However, external stimulation has not been incorporated in these models. A more comprehensive picture of signaling dynamics regulating cell polarization and movement will likely integration of all these aspects of the system.

Because of its simplicity, our model cannot account for some aspects of the chemotactic responses. It is known that latA treatment leads to suspended spherical cells that have minimal F-actin activity. When we substantially reduce the positive feedback from PIP₃ to PI3K localization, the spatial sensitivity is diminished, but is recovered when we adjust system parameters so that the system relies on the positive feedback between PTEN and PIP₂. It may be possible to obtain a parameter set which fully utilizes both feedback loops so that the system remains highly sensitive to spatial gradients even when the F-actin activity is severely reduced. Furthermore, the F-actin branching process possesses intrinsic cooperativity and positive feedback which can provide additional amplification to the PI3K-PIP₃ feedback loop. An additional positive feedback from F-actin activity to Ras activation has been observed and can contribute to the sensitivity of the PI3K pathway. Next, after cAMP removal, *Dictyostelium* cells become insensitive to stimulation up to the previous level for several minutes. This is likely due to a negative feedback from the downstream circuit to the adaptation module. This negative feedback could also explain the transient polarity reversal observed when uniform stimulation is applied shortly after removal of a static cAMP gradient [62]. However, currently there is no plausible candidate which negatively links the downstream activities to Ras activation.

Another aspect of signaling and network dynamics that has not been addressed here concerns the role of stochastic fluctuations. We have assumed that the system is deterministic, but certainly the number of cAMP molecules near a cell fluctuates, hence the number of bound receptors and downstream components all fluctuate. Estimates reported in [2] show that if the number of molecules in a ‘capture region’ surrounding a cell is in the hundreds, which obtains at low signal levels, the fluctuations in receptor occupancy will be significant, but at high signal levels they will not be important. In any case, small numbers of molecules of components in the downstream pathway may be significant. In fact, it has been shown that the stochastic version of the actin wave model described above gives rise to most of the phenomena observed during the re-building of the actin network following treatment with latA, and this suggests that stochastic effects may be important in the random extension of pseudopods in the absence of directed signals. We are however some distance from a stochastic model that integrates signaling and

mechanics.

In summary, many aspects of the chemotaxis responses can be explained by a simple model which encompasses known interactions between components of the pathway. The model also illuminates an important role of the cell morphology in affecting how *Dictyostelium* cells react to external stimulation. It also suggests a possible function of membrane ruffles and filopodia at the leading edge of *Dictyostelium* cells. Recent studies have linked PLA2 and sGC to directional persistence [7,83], and it is possible that they are involved in formation of these irregular membrane structures. The dose-dependent polarity indicated by the model also suggests a new role of *Dictyostelium* cAMP secretion in self polarity enhancement. However, future studies are needed to understand more subtle behaviors such as the transient inverse polarization and how intracellular signaling interacts with cell movement. After all, the PI3K pathway is only one of the parallel pathways that contribute to the overall chemotactic responses. It remains to be determined how concerted activities of these pathways lead to chemotactic behaviors of *Dictyostelium* cells, and models will play an important role in understanding this.

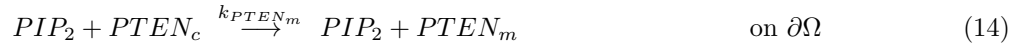
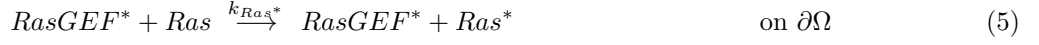
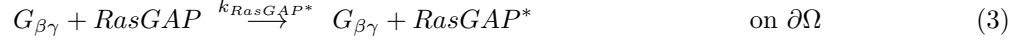
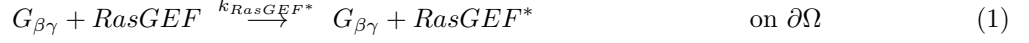
Methods

The model for PIP₃ adaptation and gradient amplification

The biochemical network underlying the model consists of an adaptation subnetwork and an amplification subnetwork, as shown in Figure 2, whose outputs are Ras activity and PIP₃ activity, respectively. The input to the model is free $G_{\beta\gamma}$ density on the membrane. For simplicity, we assume that 50%, or 1000 $\#/\mu m^2$, of total $G_{\beta\gamma}$ is free under uniform stimulation at 1 μM cAMP and that free $G_{\beta\gamma}$ density is linearly dependent on cAMP concentration [38]. Interconversion between different forms of the same molecule is denoted by solid arrows while positive regulation and promotion of a particular species and process are denoted by dashed arrows. In Figure 2, membrane-bound species are written in bold while other species are located in the cytosol. The inactive forms of RasGEF and RasGAP are part of the model but are omitted from the diagram as their conversion from active forms into inactive forms is spontaneous. In this model, all spontaneous activation and inactivation are assumed to be negligible unless these activities are important to the response. We explicitly include spontaneous activation and inactivation of Ras, which lead to polarity-induced PIP₃ localization, and spontaneous membrane binding of PI3K, which is crucial for high spatial sensitivity of the PIP₃ response. Note that contribution of these spontaneous interconversions are very small compared to that of their regulated activation and inactivation. In reality, a regulator forms a complex with its substrate before it may convert or activate the substrate. We assume for simplicity that all complex formation is fast and negligible amount of molecules is in the complex form so that the conversion rate of the substrate is proportional to the product of regulator and substrate densities. This assumption applies to membrane reactions, cytosolic reactions, and reactions at the cytosol-membrane interface. This simplification is discussed in a later section. Since diffusion of cytosolic species is significantly faster than diffusion of membrane-bound species, we assume no membrane diffusion.

The numerical simulations of model dynamics are done on 2D domains (Ω) including a circular disk and more realistic cell shapes (*cf.* Figure 7). We assume conservation of signaling molecules and that they are initially uniformly distributed. This assumption implies that the sums of active and inactive forms of RasGEF and RasGAP remain uniform throughout the simulations when the active and inactive forms diffuse equally fast. For each simulation, we apply low basal level of input, which is equivalent to 0.1 pM cAMP and allow the system to reach its equilibrium before applying stimulation. A full set of

reactions which describe our model for PIP₃ activity consists of



whose evolution can be described by a system of reaction-diffusion equations

$$\begin{aligned}
\frac{\partial RasGEF^*}{\partial t} &= D_{RasGEF} \nabla^2 RasGEF^* - k_{RasGEF} RasGEF^* && \text{in } \Omega \\
\frac{\partial RasGAP^*}{\partial t} &= D_{RasGAP} \nabla^2 RasGAP^* - k_{RasGAP} RasGAP^* && \text{in } \Omega \\
\frac{\partial PI3K_c}{\partial t} &= D_{PI3K} \nabla^2 PI3K_c && \text{in } \Omega \\
\frac{\partial PTEN_c}{\partial t} &= D_{PTEN} \nabla^2 PTEN_c && \text{in } \Omega \\
\frac{\partial Ras^*}{\partial t} &= (k_{Ras^*} RasGEF^* + k_{s,Ras^*}) \cdot Ras - (k_{Ras} RasGAP^* + k_{s,Ras}) \cdot Ras^* && \text{on } \partial\Omega \\
\frac{\partial PI3K_m}{\partial t} &= \delta k_{b,PI3K_m} PI3K_c + k_{PI3K_m} PIP_3 \cdot PI3K_c + k_{d,PI3K_m} PI3K_m^* \\
&\quad - k_{PI3K_m^*} Ras^* \cdot PI3K_m - k_{PI3K_c} PI3K_m && \text{on } \partial\Omega \\
\frac{\partial PI3K_m^*}{\partial t} &= k_{PI3K_m^*} Ras^* \cdot PI3K_m - k_{d,PI3K_m} PI3K_m^* && \text{on } \partial\Omega \\
\frac{\partial PTEN_m}{\partial t} &= k_{PTEN_m} PIP_2 \cdot PTEN_c - k_{PTEN_c} PTEN_m && \text{on } \partial\Omega \\
\frac{\partial PIP_3}{\partial t} &= k_{PIP_3} PI3K_m^* \cdot PIP_2 - k_{PIP_2} PTEN_m \cdot PIP_3 && \text{on } \partial\Omega
\end{aligned}$$

with the following boundary conditions for the cytosolic species

$$\begin{aligned}
D_{RasGEF} \frac{\partial RasGEF^*}{\partial n} &= k_{RasGEF^*} G_{\beta\gamma} \cdot RasGEF \\
D_{RasGAP} \frac{\partial RasGAP^*}{\partial n} &= k_{RasGAP^*} G_{\beta\gamma} \cdot RasGAP \\
D_{PI3K} \frac{\partial PI3K_c}{\partial n} &= k_{PI3K_c} PI3K_m - k_{PI3K_m} PIP_3 \cdot PI3K_c - \delta k_{b,PI3K_m} PI3K_c \\
D_{PTEN} \frac{\partial PTEN_c}{\partial n} &= k_{PTEN_c} PTEN_m - k_{PTEN_m} PIP_2 \cdot PTEN_c
\end{aligned}$$

on $\partial\Omega$, where $\partial/\partial n$ denotes the outward normal derivative, and conservation laws

$$\begin{aligned}
RasGEF + RasGEF^* &= RasGEF_0 && \text{in } \Omega \\
RasGAP + RasGAP^* &= RasGAP_0 && \text{in } \Omega \\
Ras + Ras^* &= Ras_0 && \text{on } \partial\Omega \\
PIP_2 + PIP_3 &= P_0 && \text{on } \partial\Omega
\end{aligned}$$

The justification for the form of the boundary conditions for RasGEF* and RasGAP* is given in the following section.

Simplification of membrane activation of cytosolic species

We begin with a full description for RasGEF activity, which involves the spontaneous deactivation in the cytosol.

$$\begin{aligned}\frac{\partial RasGEF^*}{\partial t} &= D_{RasGEF} \nabla^2 RasGEF^* - k_{RasGEF} RasGEF^* \\ \frac{\partial RasGEF}{\partial t} &= D_{RasGEF} \nabla^2 RasGEF + k_{RasGEF} RasGEF^*\end{aligned}$$

in Ω with boundary conditions

$$\begin{aligned}D_{RasGEF} \frac{\partial RasGEF}{\partial n} &= -k_b G_{\beta\gamma} \cdot RasGEF + k_{ub} [G_{\beta\gamma} RasGEF] \\ D_{RasGEF} \frac{\partial RasGEF^*}{\partial n} &= k_{act} [G_{\beta\gamma} RasGEF]\end{aligned}$$

on $\partial\Omega$. These equations account for binding to and activation by $G_{\beta\gamma}$ and the dynamics of the membrane complex, given by

$$\frac{d[G_{\beta\gamma} RasGEF]}{dt} = k_b G_{\beta\gamma} \cdot RasGEF - (k_{ub} + k_{act}) [G_{\beta\gamma} RasGEF]$$

on $\partial\Omega$. If we assume that the complex is in a quasi steady state, i.e. $\frac{d[G_{\beta\gamma} RasGEF]}{dt} = 0$, then we have

$$[G_{\beta\gamma} RasGEF] = \frac{k_b}{k_{ub} + k_{act}} G_{\beta\gamma} \cdot RasGEF$$

and

$$D_{RasGEF} \frac{\partial RasGEF}{\partial n} = -D_{RasGEF} \frac{\partial RasGEF^*}{\partial n} = -\frac{k_b k_{act}}{k_{ub} + k_{act}} G_{\beta\gamma} \cdot RasGEF$$

By defining $k_{RasGEF^*} = \frac{k_b k_{act}}{k_{ub} + k_{act}}$, we obtain the simplified form used in the model. A similar analysis applies to GAP*.

Parameters and details of the simulations

Parameters used in the simulations are listed in Table 1. The surface densities of the membrane species in the model are taken from the literature. Typical values of concentrations and diffusion constants, which are $0.1 \mu M$ and $10 \mu m^2/s$, respectively, are used for the cytosolic species. The reaction-rate constants are chosen to match experimentally-observed dynamics. In particular, the dynamics of the cytosolic Ras-binding domain (RBD) reported in [24] is used to match the responses at different levels of uniform stimulation, while the responses to static cAMP gradients are matched with the dynamics of PH_{Crac}-GFP,

a PIP₃ reporter, at the front and the back of a live cell [29]. The RBD dynamics is described by

$$\begin{aligned}
\frac{\partial RBD_c}{\partial t} &= D_{RBD} \nabla^2 RBD_c && \text{in } \Omega \\
D_{RBD} \frac{\partial RBD_c}{\partial n} &= k_{RBD_c} RBD_m - k_{RBD_m} Ras^* \cdot RBD_c && \text{on } \partial\Omega \\
\frac{\partial RBD_m}{\partial t} &= k_{RBD_m} Ras^* \cdot RBD_c - k_{RBD_c} RBD_m && \text{on } \partial\Omega
\end{aligned}$$

with the following parameters: $D_{RBD} = 10 \mu m^2/s$, $RBD_0 = 0.1 \mu M$, $k_{RBD_c} = 7.5 s^{-1}$, and $k_{RBD_m} = 1200 \mu M^{-1}s^{-1}$.

The system is solved numerically on two-dimensional domains by a finite element method with backward differentiation formula for time stepping, which is implemented in the COMSOL Multiphysics package. For each simulation, the system is first simulated with uniform basal cAMP concentration until it reaches a steady state. Then a stimulus is introduced by changing the external cAMP profile. The cAMP level is represented by the surface density of free $G_{\beta\gamma}$, which is the forcing function of the system. We assume that the free $G_{\beta\gamma}$ density is proportional to the cAMP level and that half of the heterotrimeric G protein on the membrane (with the total density of $2000 \#/\mu m^2$ [38]) is activated at $1 \mu M$ cAMP.

Adaptation of Ras activity with positive feedback from F-actin

In this section we show that Ras activity still adapts under positive feedback from F-actin under mild assumptions, given that the activation via cAMP and F-actin is independent. Note that here we only give an analysis for the local dynamics and assume that spontaneous activation and inactivation of Ras are negligible.

Suppose that Ras can be activated at two sites via cAMP and F-actin, respectively and that these activations are independent, *i.e.* the activation state at one site does not affect the activation/deactivation rates at the other site. The activation diagram of Ras is shown in Figure 14 where A is F-actin concentration.

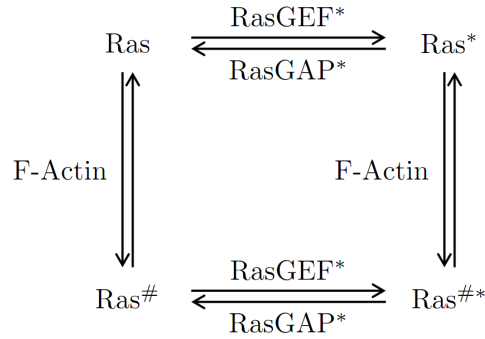


Figure 14. An adapting Ras activation model with positive feedback from F-actin.

The dynamics of Ras is given by

$$\begin{aligned}
 \frac{dRas}{dt} &= -k_{Ras^\#} A \cdot Ras - k_{Ras^*} RasGEF^* \cdot Ras + k_{Ras,A} Ras^\# + k_{Ras} RasGAP^* \cdot Ras^* \\
 \frac{dRas^\#}{dt} &= k_{Ras^\#} A \cdot Ras + k_{Ras} RasGAP^* \cdot Ras^{\#\#} - k_{Ras,A} Ras^\# - k_{Ras^*} RasGEF^* \cdot Ras^\# \\
 \frac{dRas^*}{dt} &= k_{RasGEF^*} RasGEF^* \cdot Ras + k_{Ras,A} Ras^{\#\#} - k_{Ras} RasGAP^* \cdot Ras^* - k_{Ras^\#} A \cdot Ras^* \\
 \frac{dRas^{\#\#}}{dt} &= -k_{Ras,A} Ras^{\#\#} - k_{Ras} RasGAP^* \cdot Ras^{\#\#} + k_{Ras^\#} A \cdot Ras^* + k_{Ras^*} RasGEF^* \cdot Ras^\#
 \end{aligned}$$

where we have conservation $Ras_{total} = Ras + Ras^\# + Ras^* + Ras^{\#\#}$. At steady state we have

$$\begin{bmatrix} k_{Ras,A} + k_{Ras^*} RasGEF^* & 0 & -k_{Ras} RasGAP^* \\ 0 & k_{Ras} RasGAP^* + k_{Ras^\#} A & -k_{Ras,A} \\ -k_{Ras^*} RasGEF^* & -k_{Ras^\#} A & k_{Ras,A} + k_{Ras} RasGAP^* \end{bmatrix} \begin{bmatrix} Ras^\# \\ Ras^* \\ Ras^{\#\#} \end{bmatrix} = \begin{bmatrix} k_{Ras^\#} A \cdot Ras \\ k_{Ras^*} RasGEF^* \cdot Ras \\ 0 \end{bmatrix}$$

So

$$\begin{bmatrix} Ras^\# \\ Ras^* \\ Ras^{\#\#} \end{bmatrix} = Ras \begin{bmatrix} (k_{Ras^\#}/k_{Ras,A})A \\ (k_{Ras^*}/k_{Ras})RasGEF^*/RasGAP^* \\ (k_{Ras^\#}k_{Ras^*}/k_{Ras,A}k_{Ras})A \cdot RasGEF^*/RasGAP^* \end{bmatrix}$$

and

$$Ras = \frac{Ras_{total}}{(1 + (k_{Ras\#}/k_{Ras,A})A) (1 + (k_{Ras^*}/k_{Ras})RasGEF^*/RasGAP^*)}$$

Assume that $RasGEF^*/RasGAP^* = c$ is a constant at steady state independently of cAMP concentration. Then

$$\begin{bmatrix} Ras \\ Ras\# \\ Ras^* \\ Ras\#\#^* \end{bmatrix} = \frac{Ras_{total}}{(1 + (k_{Ras\#}/k_{Ras,A})A) (1 + (k_{Ras^*}/k_{Ras})c)} \begin{bmatrix} 1 \\ (k_{Ras\#}/k_{Ras,A})A \\ (k_{Ras^*}/k_{Ras})c \\ (k_{Ras\#}k_{Ras^*}/k_{Ras,A}k_{Ras})cA \end{bmatrix}$$

Therefore, a downstream activity of Ras $f(Ras, Ras\#, Ras^* Ras\#\#^*)$ is dependent on the positive feedback from F-actin but not on cAMP concentration.

The effect of cell shape on activity of membrane-activated proteins

An infinite strip

Consider activity of a protein which is activated at the boundary of a infinite strip of $[0, L] \times \mathcal{R}$ and spontaneously deactivated within the domain

$$\begin{aligned} \frac{\partial E^*}{\partial t} &= D \nabla^2 E^* - k_1 E^*, \quad \text{in } (0, L) \times \mathcal{R} \\ D \frac{\partial E^*}{\partial n} &= k_2 S(E_0 - E^*), \quad \text{on } \{0, L\} \times \mathcal{R} \end{aligned}$$

We want to solve for the steady-state enzyme activity at the membrane. First, we can normalize the length $\theta = x/L$ so that the normalized domain is $[0, 1] \times \mathcal{R}$ and D and k_2 are replaced by $D^+ = D/L^2$ and $k_2^+ = k_2/L$. Since the problem is symmetric along the y -axis, $\partial E^*/\partial y = 0$ and we can omit dependence on y . At the steady-state we have

$$D^+ \frac{\partial^2 E^*}{\partial \theta^2} = k_1 E^*, \quad \text{in } \theta \in (0, 1)$$

whose solution is

$$E^* = c_1 \cosh(\theta/L_d^+) + c_2 \sinh(\theta/L_d^+)$$

with

$$\frac{\partial E^*}{\partial x} = \frac{1}{L_d^+} (c_1 \sinh(\theta/L_d^+) + c_2 \cosh(\theta/L_d^+))$$

where $L_d^+ = \sqrt{\frac{D^+}{k_1}}$ is normalized characteristic degradation length. We assume symmetry across the midline, and then the boundary conditions are

$$\begin{aligned} -\frac{D^+}{L_d^+} c_2 &= k_2^+ S(E_0 - c_1) \\ \frac{D^+}{L_d^+} (c_1 \sinh(1/L_d^+) + c_2 \cosh(1/L_d^+)) &= k_2^+ S(E_0 - c_1) \end{aligned}$$

at $\theta = 0, 1$ respectively. Hence

$$\begin{aligned} c_1 &= E_0 \left/ \left(1 + \frac{D^+}{k_2^+ L_d^+ S} \frac{\sinh(1/L_d^+)}{1 + \cosh(1/L_d^+)} \right) \right. \\ c_2 &= -E_0 \left/ \left(\frac{1 + \cosh(1/L_d^+)}{\sinh(1/L_d^+)} + \frac{D^+}{k_2^+ L_d^+ S} \right) \right. \end{aligned}$$

Define $L_a^+ = \frac{D^+}{k_2^+ S}$ as normalized characteristic activation length. Then

$$E^*(\theta) = \left(\frac{E_0}{1 + \frac{L_a^+}{L_d^+} \frac{\sinh(1/L_d^+)}{1 + \cosh(1/L_d^+)}} \right) \left(\cosh(\theta/L_d^+) - \frac{\sinh(1/L_d^+)}{1 + \cosh(1/L_d^+)} \sinh(\theta/L_d^+) \right)$$

The activity at either boundary ($\theta = 0, 1$) is

$$E^* = E_0 / \left(1 + \frac{L_a^+}{L_d^+} \frac{\sinh(1/L_d^+)}{1 + \cosh(1/L_d^+)} \right)$$

3D shell

Next, consider activity of the membrane-activated protein in a 3D shell $\Omega = \{(x, y, z) \in \mathcal{R}^3 \mid l \leq x^2 + y^2 + z^2 \leq L\}$. The activity is described by

$$\begin{aligned} \frac{\partial E^*}{\partial t} &= D \nabla^2 E^* - k_1 E^*, \quad \text{in } \Omega \\ D \frac{\partial E^*}{\partial n} &= k_2 S (E_0 - E^*), \quad \text{on } \partial \Omega \end{aligned}$$

In spherical coordinates, we have at steady state, by radial symmetry,

$$\frac{1}{r^2} \frac{\partial}{\partial r} \left(r^2 \frac{\partial E^*}{\partial r} \right) = k_1 E^*, \quad \text{in } r \in (l, L)$$

Following [90], let

$$f = r E^*$$

so that

$$f_{rr} = \frac{k_1}{D} f = f/L_d^2,$$

where $L_d = \sqrt{D/k_1}$ is the characteristic degradation length, which leads to a general solution

$$E^* = \frac{1}{r} (c_1 \cosh(r/L_d) + c_2 \sinh(r/L_d))$$

with

$$\frac{\partial E^*}{\partial r} = \frac{1}{r^2} \left(c_1 \left[\frac{r}{L_d} \sinh(r/L_d) - \cosh(r/L_d) \right] + c_2 \left[\frac{r}{L_d} \cosh(r/L_d) - \sinh(r/L_d) \right] \right)$$

Recall boundary conditions

$$\begin{aligned} -\frac{\partial E^*}{\partial r}(l) &= \frac{1}{L_a} (E_0 - E^*(l)) \\ \frac{\partial E^*}{\partial r}(L) &= \frac{1}{L_a} (E_0 - E^*(L)) \end{aligned}$$

where $L_a = D/k_2S$ is the characteristic activation length. Substitution gives

$$c_1 = \frac{E_0}{L_a \Pi} \left[\frac{Ll}{L_d} (l \cosh(L/L_d) + L \cosh(l/L_d)) + \frac{Ll}{L_a} (l \sinh(L/L_d) - L \sinh(l/L_d)) - l^2 \sinh(L/L_d) - L^2 \sinh(l/L_d) \right]$$

$$c_2 = \frac{E_0}{L_a \Pi} \left[-\frac{Ll}{L_d} (l \sinh(L/L_d) + L \sinh(l/L_d)) - \frac{Ll}{L_a} (l \cosh(L/L_d) - L \cosh(l/L_d)) + l^2 \cosh(L/L_d) + L^2 \cosh(l/L_d) \right]$$

where

$$\Pi = \frac{Ll}{L_d} \left[\frac{1}{L_a} \cosh((L-l)/L_d) + \frac{1}{L_d} \sinh((L-l)/L_d) \right] + \frac{Ll}{L_a} \left[\frac{1}{L_d} \cosh((L-l)/L_d) + \frac{1}{L_a} \sinh((L-l)/L_d) \right]$$

$$+ (L-l) \left[\frac{1}{L_d} \cosh((L-l)/L_d) + \frac{1}{L_a} \sinh((L-l)/L_d) \right] - \sinh((L-l)/L_d)$$

and

$$E^*(r) = \frac{E_0}{L_a \Pi r} \left\{ \frac{Ll}{L_d} [l \cosh((L-r)/L_d) + L \cosh((r-l)/L_d)] + \frac{Ll}{L_a} [l \sinh((L-r)/L_d) + L \sinh((r-l)/L_d)] \right.$$

$$\left. - l^2 \sinh((L-r)/L_d) + L^2 \sinh((r-l)/L_d) \right\}$$

The expression can be simplified as

$$E^*(r) = \begin{cases} \frac{E_0}{L_a r} \frac{K Ll [l \cosh((L-r)/L_d + \phi) + L \cosh((r-l)/L_d + \phi)] - l^2 \sinh((L-r)/L_d) + L^2 \sinh((r-l)/L_d)}{K^2 Ll \sinh((L-l)/L_d + 2\phi) + K(L-l) \cosh((L-l)/L_d + \phi) - \sinh((L-l)/L_d)} & \text{for } L_d < L_a \\ \frac{E_0}{L_a r} \frac{(Ll/L_d) [l e^{(L-r)/L_d} + L e^{(r-l)/L_d}] - l^2 \sinh((L-r)/L_d) + L^2 \sinh((r-l)/L_d)}{2(Ll/L_d^2) e^{(L-l)/L_d} + ((L-l)/L_d) e^{(L-l)/L_d} - \sinh((L-l)/L_d)} & \text{for } L_d = L_a \\ \frac{E_0}{L_a r} \frac{K Ll [l \sinh((L-r)/L_d + \phi) + L \sinh((r-l)/L_d + \phi)] - l^2 \sinh((L-r)/L_d) + L^2 \sinh((r-l)/L_d)}{K^2 Ll \sinh((L-l)/L_d + 2\phi) + K(L-l) \sinh((L-l)/L_d + \phi) - \sinh((L-l)/L_d)} & \text{for } L_d > L_a \end{cases}$$

where

$$K = \sqrt{\left| \frac{1}{L_d^2} - \frac{1}{L_a^2} \right|} \quad \text{and} \quad \phi = \begin{cases} \tanh^{-1}(L_d/L_a) & \text{for } L_d < L_a \\ \tanh^{-1}(L_a/L_d) & \text{for } L_d > L_a \end{cases}$$

Acknowledgements

We are grateful to Benjamin Jordan for a careful critique of the manuscript.

References

1. Othmer HG, Xin X, Xue C (2013) Excitation and adaptation in bacteria—a model signal transduction system that controls taxis and spatial pattern formation. *International journal of molecular sciences* 14: 9205–9248.

2. Othmer H, Schaap P (1998) Oscillatory cAMP signaling in the development of *Dictyostelium discoideum*. *Comments on Theoretical Biology* 5: 175–282.
3. Soll DR, Wessels D, Sylwester A (1993) The motile behavior of amoebae in the aggregation wave in *Dictyostelium discoideum*. In: Othmer HG, Maini PK, Murray JD, editors, *Experimental and Theoretical Advances in Biological Pattern Formation*. London: Plenum, pp. 325–338.
4. Soll DR (1995) The use of computers in understanding how animal cells crawl. In: Jeon KW, Jarvik J, editors, *International Review of Cytology*, Academic Press, volume 163. pp. 43–104.
5. Haastert PJMV, Devreotes PN (2004) Chemotaxis: signalling the way forward. *Nat Rev Mol Cell Biol* 5: 626–634.
6. Li L, Nrelykke SF, Cox EC (2008) Persistent cell motion in the absence of external signals: a search strategy for eukaryotic cells. *PLoS One* 3: e2093.
7. Bosgraaf L, Haastert PJMV (2009) The ordered extension of pseudopodia by amoeboid cells in the absence of external cues. *PLoS One* 4: e5253.
8. McRobbie S, Newell P (1983) Changes in actin associated with the cytoskeleton following chemotactic stimulation of *dictyostelium discoideum*. *Biochemical and biophysical research communications* 115: 351–359.
9. Condeelis J, et al. (1990) Mechanisms of ameboid chemotaxis: An evaluation of the cortical expansion model. *Developmental Genetics* 11: 333–340.
10. Varnum B, Edwards KB, Soll DR (1985) *Dictyostelium* amebae alter motility differently in response to increasing versus decreasing temporal gradients of cAMP 101: 1–5.
11. Wessels D, Murray J, Soll DR (1992) Behavior of *Dictyostelium* amoebae is regulated primarily by the temporal dynamic of the natural cAMP wave. *Cell Motil Cytoskeleton* 23: 145–156.
12. Zigmond SH (1977) Ability of polymorphonuclear leukocytes to orient in gradients of chemotactic factors. *J Cell Biol* 75: 606–616.
13. Kriebel PW, Barr VA, Parent CA (2003) Adenylyl cyclase localization regulates streaming during chemotaxis. *Cell* 112: 549–560.
14. Swanson J, Taylor DL (1982) Local and spatially coordinated movements in *Dictyostelium discoideum* amoebae during chemotaxis 28: 225–232.
15. Alcantara F, Monk M (1974) Signal propagation during aggregation in the slime mold *Dictyostelium discoideum*. *J Gen Microbiol* 85: 321–334.
16. Meier B, Zielinski A, Weber C, Arcizet D, Youssef S, et al. (2011) Chemotactic cell trapping in controlled alternating gradient fields. *Proc Natl Acad Sci U S A* 108: 11417–11422.

17. Parent CA, Devreotes PN (1999) A cell's sense of direction. *Science* 284: 765–770.
18. Gerisch G (1982) Chemotaxis in *Dictyostelium* 44: 535–552.
19. Andrew N, Insall RH (2007) Chemotaxis in shallow gradients is mediated independently of PtdIns 3-kinase by biased choices between random protrusions. *Nat Cell Biol* 9: 193–200.
20. Fisher PR, Merkl R, Gerisch G (1989) Quantitative analysis of cell motility and chemotaxis in *Dictyostelium discoideum* by using an image processing system and a novel chemotaxis chamber providing stationary chemical gradients. *J Cell Biol* 108: 973–984.
21. Brenner M, Thomas SD (1984) Caffeine blocks activation of cyclic AMP synthesis in *dictyostelium discoideum*. *Dev Biol* 101: 136–146.
22. Siegert F, Weijer CJ (1989) Digital image processing of optical density wave propagation in *Dictyostelium discoideum* and analysis of the effects of caffeine and ammonia 93: 325–335.
23. Parent CA, Blacklock BJ, Froehlich WM, Murphy DB, Devreotes PN (1998) G protein signaling events are activated at the leading edge of chemotactic cells. *Cell* 95: 81–91.
24. Takeda K, Shao D, Adler M, Charest PG, Loomis WF, et al. (2012) Incoherent feedforward control governs adaptation of activated Ras in a eukaryotic chemotaxis pathway. *Sci Signal* 5: ra2.
25. Tang Y, Othmer HG (1995) Excitation, oscillations and wave propagation in a G-protein-based model of signal transduction in *Dictyostelium discoideum*. *Philos Trans R Soc Lond B Biol Sci* 349: 179–195.
26. Dallon JC, Othmer HG (1998) A continuum analysis of the chemotactic signal seen by *Dictyostelium discoideum*. *J Theor Biol* 194: 461–483.
27. Chen L, Janetopoulos C, Huang YE, Iijima M, Borleis J, et al. (2003) Two phases of actin polymerization display different dependencies on PI(3,4,5)P₃ accumulation and have unique roles during chemotaxis. *Mol Biol Cell* 14: 5028–5037.
28. Sasaki AT, Chun C, Takeda K, Firtel RA (2004) Localized Ras signaling at the leading edge regulates PI3K, cell polarity, and directional cell movement. *J Cell Biol* 167: 505–518.
29. Xu X, Meier-Schellersheim M, Jiao X, Nelson LE, Jin T (2005) Quantitative imaging of single live cells reveals spatiotemporal dynamics of multistep signaling events of chemoattractant gradient sensing in *Dictyostelium*. *Mol Biol Cell* 16: 676–688.
30. Kortholt A, Kataria R, Keizer-Gunnink I, Egmond WNV, Khanna A, et al. (2011) *Dictyostelium* chemotaxis: essential Ras activation and accessory signalling pathways for amplification. *EMBO Rep* 12: 1273–1279.
31. Zhang S, Charest PG, Firtel RA (2008) Spatiotemporal regulation of Ras activity provides directional sensing. *Curr Biol* 18: 1587–1593.

32. Funamoto S, Milan K, Meili R, Firtel RA (2001) Role of phosphatidylinositol 3' kinase and a downstream pleckstrin homology domain-containing protein in controlling chemotaxis in dictyostelium. *J Cell Biol* 153: 795–810.
33. Afonso PV, Parent CA (2011) Pi3k and chemotaxis: a priming issue? *Sci Signal* 4: pe22.
34. Sasaki AT, Janetopoulos C, Lee S, Charest PG, Takeda K, et al. (2007) G protein-independent Ras/PI3K/F-actin circuit regulates basic cell motility. *J Cell Biol* 178: 185–191.
35. Welf ES, Ahmed S, Johnson HE, Melvin AT, Haugh JM (2012) Migrating fibroblasts reorient directionality by a metastable, pi3k-dependent mechanism. *J Cell Biol* 197: 105–114.
36. Goldbeter A, Segel LA (1977) Unified mechanism for relay and oscillation of cyclic amp in dictyostelium discoideum. *Proc Natl Acad Sci U S A* 74: 1543–1547.
37. Meinhardt H (1999) Orientation of chemotactic cells and growth cones: models and mechanisms. *J Cell Sci* 112 (Pt 17): 2867–2874.
38. Meier-Schellersheim M, Xu X, Angermann B, Kunkel EJ, Jin T, et al. (2006) Key role of local regulation in chemosensing revealed by a new molecular interaction-based modeling method. *PLoS Comput Biol* 2: e82.
39. Xiong Y, Huang CH, Iglesias PA, Devreotes PN (2010) Cells navigate with a local-excitation, global-inhibition-biased excitable network. *Proc Natl Acad Sci U S A* 107: 17079–17086.
40. Gierer A, Meinhardt H (1972) A theory of biological pattern formation. *Biological Cybernetics* 12: 30–39.
41. Shi C, Huang CH, Devreotes PN, Iglesias PA (2013) Interaction of motility, directional sensing, and polarity modules recreates the behaviors of chemotaxing cells. *PLOS Computational Biology* 9: e1003122.
42. Gamba A, de Candia A, Talia SD, Coniglio A, Bussolino F, et al. (2005) Diffusion-limited phase separation in eukaryotic chemotaxis. *Proc Natl Acad Sci U S A* 102: 16927–16932.
43. Mori Y, Jilkine A, Edelstein-Keshet L (2008) Wave-pinning and cell polarity from a bistable reaction-diffusion system. *Biophys J* 94: 3684–3697.
44. Hecht I, Kessler DA, Levine H (2010) Transient localized patterns in noise-driven reaction-diffusion systems. *Phys Rev Lett* 104: 158301.
45. Jilkine A, Edelstein-Keshet L (2011) A comparison of mathematical models for polarization of single eukaryotic cells in response to guided cues. *PLoS Comput Biol* 7: e1001121.
46. Levchenko A, Iglesias PA (2002) Models of eukaryotic gradient sensing: application to chemotaxis of amoebae and neutrophils. *Biophys J* 82: 50–63.

47. Kortholt A, van Haastert PJM (2008) Highlighting the role of Ras and Rap during Dictyostelium chemotaxis. *Cell Signal* 20: 1415–1422.
48. Kataria R, Xu X, Fusetti F, Keizer-Gunnink I, Jin T, et al. (2013) Dictyostelium ric8 is a nonreceptor guanine exchange factor for heterotrimeric G proteins and is important for development and chemotaxis. *Proc Natl Acad Sci U S A* 110: 6424–6429.
49. Wilkins A, Szafranski K, Fraser DJ, Bakthavatsalam D, Muller R, et al. (2005) The dictyostelium genome encodes numerous rasGEFs with multiple biological roles. *Genome Biol* 6: R68.
50. Kae H, Kortholt A, Rehmann H, Insall RH, Haastert PJMV, et al. (2007) Cyclic AMP signalling in Dictyostelium: G-proteins activate separate Ras pathways using specific RasGEFs. *EMBO Rep* 8: 477–482.
51. Funamoto S, Meili R, Lee S, Parry L, Firtel RA (2002) Spatial and temporal regulation of 3-phosphoinositides by PI 3-kinase and PTEN mediates chemotaxis. *Cell* 109: 611–623.
52. Bolourani P, Spiegelman GB, Weeks G (2008) Rap1 activation in response to cAMP occurs downstream of Ras activation during Dictyostelium aggregation. *J Biol Chem* 283: 10232–10240.
53. Charest PG, Shen Z, Lakoduk A, Sasaki AT, Briggs SP, et al. (2010) A Ras signaling complex controls the RasC-TORC2 pathway and directed cell migration. *Dev Cell* 18: 737–749.
54. Park KC, Rivero F, Meili R, Lee S, Apone F, et al. (2004) Rac regulation of chemotaxis and morphogenesis in Dictyostelium. *EMBO J* 23: 4177–4189.
55. Han JW, Leeper L, Rivero F, Chung CY (2006) Role of RacC for the regulation of WASP and phosphatidylinositol 3-kinase during chemotaxis of Dictyostelium. *J Biol Chem* 281: 35224–35234.
56. Yan J, Mihaylov V, Xu X, Brzostowski JA, Li H, et al. (2012) A $G\beta\gamma$ Effector, ElmoE, Transduces GPCR Signaling to the Actin Network during Chemotaxis. *Dev Cell* 22: 92–103.
57. Loovers HM, Postma M, Keizer-Gunnink I, Huang YE, Devreotes PN, et al. (2006) Distinct roles of PI(3,4,5)P₃ during chemoattractant signaling in Dictyostelium: a quantitative in vivo analysis by inhibition of PI3-kinase. *Mol Biol Cell* 17: 1503–1513.
58. Kortholt A, Rehmann H, Kae H, Bosgraaf L, Keizer-Gunnink I, et al. (2006) Characterization of the GbpD-activated Rap1 pathway regulating adhesion and cell polarity in Dictyostelium discoideum. *J Biol Chem* 281: 23367–23376.
59. Jeon TJ, Lee DJ, Lee S, Weeks G, Firtel RA (2007) Regulation of Rap1 activity by RapGAP1 controls cell adhesion at the front of chemotaxing cells. *J Cell Biol* 179: 833–843.
60. Kortholt A, Bolourani P, Rehmann H, Keizer-Gunnink I, Weeks G, et al. (2010) A Rap/phosphatidylinositol 3-kinase pathway controls pseudopod formation. *Mol Biol Cell* 21: 936–945.

61. Janetopoulos C, Jin T, Devreotes P (2001) Receptor-mediated activation of heterotrimeric G-proteins in living cells. *Science* 291: 2408–2411.
62. Xu X, Meier-Schellersheim M, Yan J, Jin T (2007) Locally controlled inhibitory mechanisms are involved in eukaryotic GPCR-mediated chemosensing. *J Cell Biol* 178: 141–153.
63. Khamviwath V, Othmer HG (2013) Modular analysis of signal transduction networks. In preparation.
64. Weiner OD, Neilsen PO, Prestwich GD, Kirschner MW, Cantley LC, et al. (2002) A ptdinsp(3)- and rho gtpase-mediated positive feedback loop regulates neutrophil polarity. *Nat Cell Biol* 4: 509–513.
65. Postma M, Roelofs J, Goedhart J, Loovers HM, Visser AJWG, et al. (2004) Sensitization of Dictyostelium chemotaxis by phosphoinositide-3-kinase-mediated self-organizing signalling patches. *J Cell Sci* 117: 2925–2935.
66. Ferguson GJ, Milne L, Kulkarni S, Sasaki T, Walker S, et al. (2007) Pi(3)kgamma has an important context-dependent role in neutrophil chemokinesis. *Nat Cell Biol* 9: 86–91.
67. Khamviwath V, Hu J, Othmer HG (2013) A continuum model of actin waves in dictyostelium discoideum. *PLoS One* 8: e64272.
68. Hoeller O, Kay RR (2007) Chemotaxis in the absence of PIP3 gradients. *Curr Biol* 17: 813–817.
69. Schneider IC, Parrish EM, Haugh JM (2005) Spatial analysis of 3' phosphoinositide signaling in living fibroblasts, iii: influence of cell morphology and morphological polarity. *Biophys J* 89: 1420–1430.
70. Krishnan J, Iglesias PA (2007) Receptor-mediated and intrinsic polarization and their interaction in chemotaxing cells. *Biophys J* 92: 816–830.
71. Hecht I, Skoge ML, Charest PG, Ben-Jacob E, Firtel RA, et al. (2011) Activated membrane patches guide chemotactic cell motility. *PLoS Comput Biol* 7: e1002044.
72. Wang CJ, Bergmann A, Lin B, Kim K, Levchenko A (2012) Diverse sensitivity thresholds in dynamic signaling responses by social amoebae. *Sci Signal* 5: ra17.
73. Dinauer MC, Steck TL, Devreotes PN (1980) Cyclic 3',5'-AMP relay in Dictyostelium discoideum IV. Recovery of the cAMP signaling response after adaptation to cAMP. *J Cell Biol* 86: 545–553.
74. Machacek M, Danuser G (2006) Morphodynamic profiling of protrusion phenotypes. *Biophys J* 90: 1439–1452.
75. Houk AR, Jilkine A, Mejean CO, Boltyanskiy R, Dufresne ER, et al. (2012) Membrane tension maintains cell polarity by confining signals to the leading edge during neutrophil migration. *Cell* 148: 175–188.

76. Yoo SK, Deng Q, Cavnar PJ, Wu YI, Hahn KM, et al. (2010) Differential regulation of protrusion and polarity by pi3k during neutrophil motility in live zebrafish. *Dev Cell* 18: 226–236.
77. Gerisch G (2010) Self-organizing actin waves that simulate phagocytic cup structures. *PMC Biophys* 3: 7.
78. Arai Y, Shibata T, Matsuoka S, Sato MJ, Yanagida T, et al. (2010) Self-organization of the phosphatidylinositol lipids signaling system for random cell migration. *Proc Natl Acad Sci U S A* 107: 12399–12404.
79. Taniguchi D, Ishihara S, Oonuki T, Honda-Kitahara M, Kaneko K, et al. (2013) Phase geometries of two-dimensional excitable waves govern self-organized morphodynamics of amoeboid cells. *Proc Natl Acad Sci U S A* 110: 5016–5021.
80. Bosgraaf L, Keizer-Gunnink I, Haastert PJMV (2008) PI3-kinase signaling contributes to orientation in shallow gradients and enhances speed in steep chemoattractant gradients. *J Cell Sci* 121: 3589–3597.
81. Comer FI, Lippincott CK, Masbad JJ, Parent CA (2005) The PI3K-mediated activation of CRAC independently regulates adenylyl cyclase activation and chemotaxis. *Curr Biol* 15: 134–139.
82. Yang C, Czech L, Gerboth S, ichiro Kojima S, Scita G, et al. (2007) Novel roles of formin mDia2 in lamellipodia and filopodia formation in motile cells. *PLoS Biol* 5: e317.
83. Bosgraaf L, Haastert PJMV (2009) Navigation of chemotactic cells by parallel signaling to pseudopod persistence and orientation. *PLoS One* 4: e6842.
84. Van Haastert PJM, de Wit RJ (1984) Demonstration of receptor heterogeneity and affinity modulation by nonequilibrium binding experiments. *J of Biological Chemistry* 259: 13321–13328.
85. Berg HC, Purcell EM (1977) Physics of chemoreception. *Biophys J* 20: 193–219.
86. Van Haastert PJ (1987) Down-regulation of cell surface cyclic AMP receptors and desensitization of cyclic AMP-stimulated adenylyl cyclase by cyclic AMP in *Dictyostelium discoideum*. kinetics and concentration dependence 262: 7700–7704.
87. Eigen M, Hammes G (1963) *Advances in Enzymology*, Interscience, volume 25, chapter Elementary steps in enzyme reactions. pp. 1–38.
88. Ma L, Janetopoulos C, Yang L, Devreotes PN, Iglesias PA (2004) Two complementary, local excitation, global inhibition mechanisms acting in parallel can explain the chemoattractant-induced regulation of PI(3,4,5)P3 response in dictyostelium cells. *Biophys J* 87: 3764–3774.
89. Postma M, Van Haastert PJ (2001) A diffusion-translocation model for gradient sensing by chemotactic cells. *Biophys J* 81: 1314–1323.
90. Crank J (1956) *The Mathematics of Diffusion*. Clarendon Press.

Supporting information

Figure S1. PIP₃ localization dynamics under uniform stimulation. A resting cell is subject to $0.1 \mu M$ cAMP at $0 s$.

Figure S2. PIP₃ localization dynamics under an upward gradient. A resting cell is subject to a directional cue in the direction of the y -axis with 50% difference in cAMP levels across the cell. The mean cAMP level is $0.1 \mu M$.